nature neuroscience

Article

https://doi.org/10.1038/s41593-024-01763-8

Synergistic association of Aβ and tau pathology with cortical neurophysiology and cognitive decline in asymptomatic older adults

Received: 6 July 2023

Accepted: 13 August 2024

Published online: 18 September 2024

Check for updates

Jonathan Gallego-Rudolf[1,2], Alex I. Wiesman[2], Alexa Pichet Binette[1,3], Sylvia Villeneuve[1,2], Sylvain Baillet[2] ✉ & PREVENT-AD Research Group*

Animal and computational models of Alzheimer's disease (AD) indicate that early amyloid-β (Aβ) deposits drive neurons into a hyperactive regime, and that subsequent tau depositions manifest an opposite, suppressive effect as behavioral deficits emerge. Here we report analogous changes in macroscopic oscillatory neurophysiology in the human brain. We used positron emission tomography and task-free magnetoencephalography to test the effects of Aβ and tau deposition on cortical neurophysiology in 104 cognitively unimpaired older adults with a family history of sporadic AD. In these asymptomatic individuals, we found that Aβ depositions colocalize with accelerated neurophysiological activity. In those also presenting medial–temporal tau pathology, linear mixed effects of Aβ and tau depositions indicate a shift toward slower neurophysiological activity, which was also linked to cognitive decline. We conclude that early Aβ and tau depositions relate synergistically to human cortical neurophysiology and subsequent cognitive decline. Our findings provide insight into the multifaceted neurophysiological mechanisms engaged in the preclinical phases of AD.

The current state of knowledge suggests that the pathological processes underlying Alzheimer's disease (AD) develop along a continuum[1,2], with a prolonged preclinical phase of pathological buildup preceding detectable neurodegeneration, and cognitive symptoms manifesting in the later disease stages[3–5]. The defining histopathological hallmarks of AD are the accumulation of amyloid-β (Aβ) plaques and fibrillary tangles of hyperphosphorylated tau proteins in the brain[4,6–8]. Aβ plaques deposition can begin up to two decades before symptom onset[1,4,9], initially accumulating in cortical areas with high metabolic baseline activity, such as the precuneus, medial orbitofrontal and posterior cingulate cortices[10,11], before spreading to the entire neocortex, brainstem and subcortical nuclei[12,13]. Tau deposition also follows a relatively stereotypical distribution pattern, accumulating first in the entorhinal cortex before spreading to limbic areas and eventually the neocortex[6,14,15]. The joint accumulation of Aβ and tau triggers a cascade of deleterious events from synaptic loss, neuronal death, to brain atrophy[5,16–18], which are thought to underlie the cognitive deficits that characterize the disease[4,19]. However, the exact mechanisms behind the disruption of human neural function and cognition related to AD proteinopathy remain to be elucidated.

A plausible mechanism of these noxious effects is that the joint accumulation of Aβ and tau alters neurophysiological signaling,

[1]Douglas Research Centre, McGill University, Montreal, Quebec, Canada. [2]McConnell Brain Imaging Centre, Montreal Neurological Institute, McGill University, Montreal, Quebec, Canada. [3]Clinical Memory Research Unit, Lund University, Lund, Sweden. *A list of authors and their affiliations appears at the end of the paper. ✉e-mail: sylvain.baillet@mcgill.ca

https://doi.org/10.1038/s41593-024-01763-8

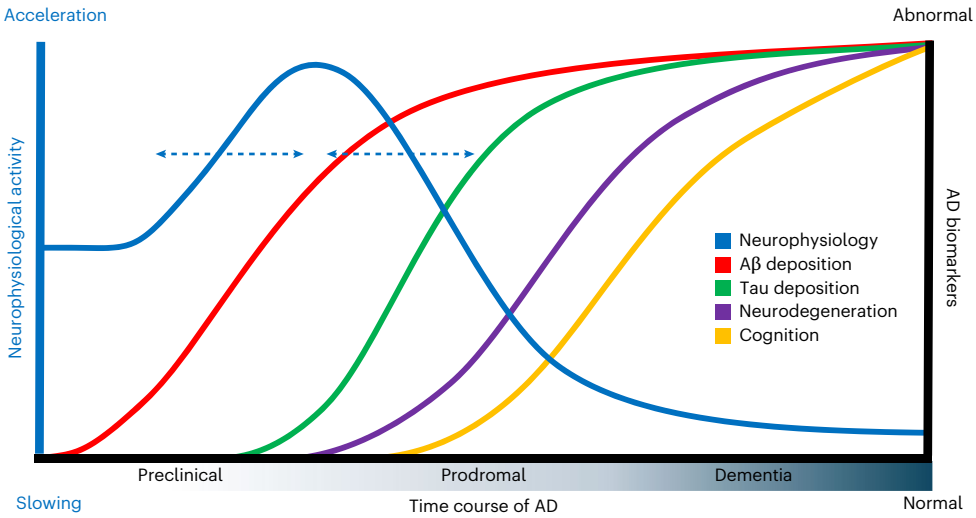

Fig. 1 | Time-course of pathological changes along the AD continuum. The traces represent the possible evolution of pathological changes across the AD continuum, with the new hypothesis of an early shift in neurophysiological activity from acceleration to slowing during the preclinical phase. Aβ deposition begins early in the preclinical stage of the disease, preceding tau deposition, subsequent neurodegeneration and presentation of cognitive symptoms. According to the proposed model, early Aβ deposition is related to a transient acceleration of neurophysiological activity, while the later joint deposition of Aβ and tau would be associated with a shift towards neurophysiological slowing. The left axis in blue corresponds to the acceleration and slowing of neurophysiological activity, while right black axis depicts more generally the nature of AD pathological changes from normal to abnormal. The double arrows highlight the uncertainty around the onset of the neurophysiological acceleration and slowing with respect to other early pathological changes.

triggering further pathological processes in a chain reaction that promotes disease progression[20,21]. Animal models show that Aβ deposition induces a toxic regime of neuronal hyperactivity, which then contributes to aggravating Aβ pathology itself[22,23]. This positive feedback process would then promote the accumulation and spread of tau pathology[20]. Consequently, the joint, colocalized accumulation of Aβ plaques and tau neurofibrillary tangles can be conceived as synergistic, potentially driving shifts in neuronal activity toward a regime of relative hypoactivity[20,24]. At this stage, neuronal activity is considerably diminished, eventually leading to cell death, tissue degeneration and severe behavioral changes[20,21,25].

Whether this hypothetical two-pronged shifting regime of neural dynamics induced by AD proteinopathy occurs at the macroscopic scale in the human brain is still debated. In the prodromal stage of AD, increased blood-oxygen-level-dependent (BOLD) activations in hippocampal and middle temporal lobe circuits have been reported in memory tasks using functional magnetic resonance imaging (fMRI)[26–28]. In contrast, BOLD responses are typically diminished during later disease stages[26,29]. Considering the magnitude of BOLD signals as a proxy of brain activation, these observations are aligned with the expected gradual shift of brain activity related to the synergistic effects of Aβ and tau pathology, along an inverted U-shape trajectory—from baseline to hyperactive then hypoactive levels across the AD continuum (Fig. 1).

Direct measurements of human brain electrophysiology also indicate aberrant macroscopic neurophysiological signaling in patients with AD-like symptoms[30–34]. A consistent observation with electroencephalography (EEG) and magnetoencephalography (MEG) is that low-frequency neurophysiological activity (delta–theta bands; 2–8 Hz) is increased and higher frequency activity (mainly in the alpha band; 8–12 Hz) is reduced in the symptomatic and prodromal stages of the disease[31,35–40].

A recent computational model of the neurophysiology of AD proteinopathies points to a possible causal effect of early Aβ and tau depositions via the disruption of the excitatory/inhibitory balance of local neuronal populations, which in turn alters the macroscopic neurophysiological frequency spectrum across brain networks in the later stages of the disease[41]. According to this model, the accumulation of Aβ and tau induces a gradual shift in neuronal activity from hyperactivity to hypoactivity with respect to baseline healthy variants, notably manifesting at the macroscopic scale with levels of alpha-band activity following an inverted U-shaped trajectory across the AD continuum. For this reason, in the present study, we map with MEG the levels of cortical alpha-band activity with respect to other typical frequency bands as a noninvasive, macroscopic proxy of relative neurophysiological acceleration/slowing effects related to AD proteinopathy.

There is early evidence of these model predictions from human empirical data, albeit still relatively limited in scope. The alpha-band activity in participants with greater Aβ deposition is increased compared to normative healthy controls, but it is reduced in patients presenting mild cognitive impairment (MCI)[42]. The same study also reported increased, slower delta-band (1–4 Hz) activity in MCI patients, which together with decreased alpha-band activity, is aligned with the prediction of an acceleration effect on oscillatory neurophysiological activity (increased alpha-band activity) followed by a shift towards neurophysiological slowing (decreased alpha-band power and increased delta-band activity) during the prodromal stage of AD, as cognitive decline starts to manifest. These observations were independently confirmed recently in reports of Aβ[33,40] and tau[32,33] accumulations, which are related to decreased alpha-band and increased delta-band activity—that is neurophysiological slowing—in the later stages of AD. Whether a more subtle neurophysiological shift from enhanced fast-frequency activity to neurophysiological slowing related to AD proteinopathy and cognitive outcomes is detectable macroscopically in the preclinical stages of the disease, when potential therapeutic interventions may have the greatest impact[39], was the overarching question of the present study.

We used task-free MEG source imaging of millisecond brain activity and whole-brain quantitative PET imaging of Aβ and tau in 104 asymptomatic older adults with familial history of sporadic AD dementia (Fig. 2a). As anticipated, we found that early Aβ deposition is associated with macroscopic neurophysiological manifestations of hyperactivity, expressed as an acceleration of neurophysiological oscillatory activity reflected by increased alpha-band and decreased delta-band activity. As predicted from disease models, we also found that these effects shift from oscillatory acceleration to slowing in individuals presenting early temporal lobe tau pathology, as denoted by decreased alpha-band and increased delta-band activity (Fig. 1). Finally, we demonstrate that the

https://doi.org/10.1038/s41593-024-01763-8

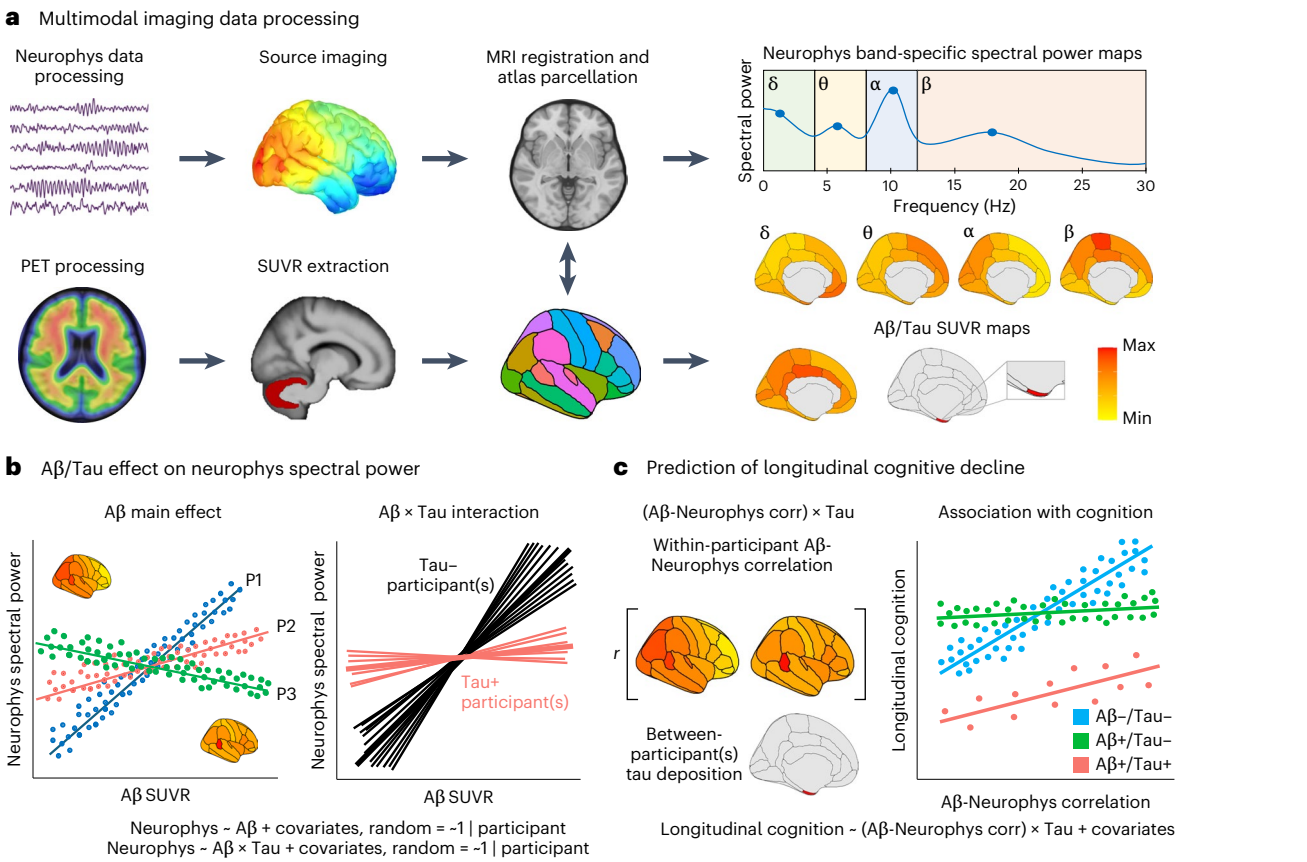

Fig. 2 | Multimodal data processing and analysis pipeline. a, Neurophysiological data were preprocessed, source imaged, frequency-transformed and averaged per canonical frequency bands (delta, 2–4 Hz; theta, 5–7 Hz; alpha, 8–12 Hz and beta, 15–29 Hz) and within each of the 68 cortical regions-of-interest (ROI) from the Desikan–Killiany atlas. PET images were preprocessed to obtain standardized uptake value ratio (SUVR) maps, which were then averaged within each cortical region of the same atlas across the whole brain (Aβ) or within temporal lobe ROIs (entorhinal cortex and temporal meta-ROI) for tau. **b**, Nested LME models were used to test for the main effect of Aβ deposition on neurophysiological activity, as well as the interactive between-participants effect of temporal tau deposition on this association. **c**, To assess impacts on cognitive performance, the correlation between Aβ and neurophysiological spectral power was estimated to test whether the interaction of this relationship with tau deposition across individuals related to longitudinal declines in attention and memory.

magnitude of the shift from neurophysiological acceleration to slowing is associated with longitudinal cognitive decline, and that the magnitude of the changes in neurophysiology and proteinopathy predicted by our model aligns with published observations in patients in the later stages of the AD continuum (that is MCI and AD).

Results

Neurophysiological shifts linked to Aβ and tau

Participant demographics and summary descriptive statistics of the PET data analyses and the screening and MEG-PET visit cognitive testing are provided in Table 1. We used ANCOVAs to compare the mean relative spectral power of whole-brain cortical neurophysiological activity across the following three PET-defined subgroups of individuals (Table 2): (1) those with no Aβ nor tau burden (Aβ−/Tau−), (2) those with high levels of global Aβ but no entorhinal tau (Aβ+/Tau−) and (3) those with both high global Aβ and high entorhinal tau (Aβ+/Tau+). In general, participants with greater levels of Aβ and tau exhibited higher levels of slow activity (delta–theta band), and lower levels of faster activity (alpha–beta band; Extended Data Fig. 1). Repeating the analysis after removing the influential cases resulted in similar associations, with significant statistical differences observed for the delta and alpha bands (Extended Data Table 1).

Table 1 | PREVENT-AD participant characteristics

PREVENT-AD sample characteristics	
Sample size	104
Age in years	67.4 (4.9)
Female, % (*n*)	71.1 (74)
Years of education	15 (3.1)
APOE ε4 carriers, % (*n*)	40.3 (42)
Global Aβ SUVR index	1.29 (0.31)
Entorhinal cortex tau SUVR	1.08 (0.13)
Temporal meta-ROI tau SUVR	1.12 (0.10)
MoCA score (baseline)	28.1 (1.5)
MMSE score (MEG–PET visit)	28.8 (1.2)

Summary of relevant metrics from the PRe-symptomatic EValuation of Experimental or Novel Treatments for Alzheimer's Disease (PREVENT-AD) participants included in this study. The table shows the key demographics, as well as the group average (and s.d.) global Aβ and temporal tau PET SUVR, baseline MoCA cognitive screening scores and global cognition MMSE scores collected around the time of the MEG–PET visit. MoCA, Montreal Cognitive Assessment; MMSE, mini-mental state examination.

Proteinopathy-related shifts in neurophysiological activity

Considering the sample size imbalance between PET subgroups and the limitations of using a positivity cutoff that ignores potentially meaningful, subthreshold levels of pathology, we implemented nested linear mixed effects models (LME) to better incorporate intra-participant spatial variability in our modeled associations between Aβ, entorhinal tau and neurophysiological activity (Fig. 2b). We found

https://doi.org/10.1038/s41593-024-01763-8

Table 2 | Whole-brain averaged between-participants spectral power analysis

Between-participants spectral power analysis								
MEG frequency band	Aβ−/Tau− mean (CI)	Aβ+/Tau− mean (CI)	Aβ+/Tau+ mean (CI)	ANCOVA *F* statistic	*P* value	Aβ−/Tau− versus Aβ+/Tau−	Aβ−/Tau− versus Aβ+/Tau+	Aβ+/Tau− versus Aβ+/Tau+
Delta-band (2–4 Hz)	0.32 (0.30–0.35)	0.29 (0.27–0.31)	0.37 (0.30–0.44)	4.58 (2,95)	**0.025**	0.119	0.244	**0.016**
Theta-band (5–7 Hz)	0.21 (0.20–0.22)	0.19 (0.19–0.20)	0.23 (0.20–0.27)	4.76 (2,95)	**0.025**	0.120	0.213	**0.013**
Alpha-band (8–12 Hz)	0.25 (0.23–0.28)	0.28 (0.26–0.31)	0.21 (0.16–0.27)	3.15 (2,95)	**0.047**	0.236	0.336	**0.054**
Beta-band (15–29 Hz)	0.11 (0.10–0.13)	0.13 (0.12–0.14)	0.09 (0.07–0.12)	3.79 (2,95)	**0.034**	0.240	0.224	**0.025**

Summary of the between-participants analysis comparing whole-brain neurophysiological activity spectral power across PET-defined groups. Values indicate the mean and confidence intervals of the relative power for each frequency band, followed by statistics from the two-sided, one-factor ANCOVA test (*F* statistic (df) and FDR corrected *P* values) and post hoc pairwise comparisons (Tukey's Honestly Significant Difference [HSD] test adjusted *P* values). Significant differences between the groups (corrected $P < 0.05$) are highlighted in bold. Aβ+/Tau+ individuals showed increased low-frequency power (delta and theta bands) and decreased fast-frequency activity (beta band and trend in alpha band), when compared to the Aβ+/Tau− individuals. CI, confidence interval.

that the regional deposition of Aβ is related to an enhancement of fast-frequency neurophysiological activity, scaling with increased alpha-band activity ($t_{(6967)} = 14.23$, $P_{FDR} = 0.016$) and decreased delta-band activity ($t_{(6967)} = -14.69$, $P_{FDR} = 0.016$). Notably, this effect was reduced in individuals with greater tau pathology in both the alpha ($t_{(6966)} = -5.46$, $P_{FDR} < 0.001$) and delta ($t_{(6966)} = 4.33$, $P_{FDR} < 0.001$) frequency bands, indicating a tau-related shift towards neurophysiological slowing (Fig. 3). The aperiodic component of the neurophysiological power spectrum did not impact the observed associations between neurophysiological activity and Aβ deposition (alpha band—$t_{(6965)} = 14.25$, $P_{FDR} = 0.008$; delta band—$t_{(6965)} = -15.76$, $P_{FDR} < 0.001$), nor their synergistic effects with entorhinal tau deposition (alpha band—$t_{(6964)} = -4.52$, $P_{FDR} < 0.001$; delta band—$t_{(6964)} = 5.54$, $P_{FDR} < 0.001$).

To ensure that the moderating effects of tau deposition on the Aβ–neurophysiological relationships are not biased by assessing tau burden from a single region-of-interest (ROI) (entorhinal cortex), we repeated the analyses after assessing tau burden across an expanded set of temporal cortical regions (temporal meta-ROI) which are widely used for assessing early tau deposition[43]. Higher temporal meta-ROI tau values also related to a shift in the association between Aβ and neurophysiological activity in the alpha ($t_{(6966)} = -4.27$, $P_{FDR} < 0.001$) and delta ($t_{(6966)} = 3.46$, $P_{FDR} = 0.004$) frequency bands, in the same opposite directions as observed with the entorhinal cortex as tau ROI (Extended Data Fig. 2). Once again, the aperiodic components of the neurophysiological power spectrum did not affect the synergistic effects of Aβ and tau on neurophysiological activity (alpha band—$t_{(6964)} = -3.31$, $P_{FDR} = 0.010$; delta band—$t_{(6964)} = 4.8$, $P_{FDR} < 0.001$). The same pattern of tau effects remained after removing the entorhinal cortex from the temporal meta-ROI (alpha band—$t_{(6966)} = -3.74$, $P_{FDR} < 0.001$; delta band—$t_{(6966)} = 3.06$, $P_{FDR} = 0.008$). A similar trend for the interactive effect of Aβ and tau on alpha-band power was observed when using whole-brain tau standardized uptake value ratio (SUVR) values as a nested variable, although these associations were no longer significant after permutation and FDR correction (alpha band—$t_{(6965)} = -6.42$, $P_{FDR} = 0.106$; delta band—$t_{(6965)} = 2.67$, $P_{FDR} = 0.296$; Extended Data Fig. 2).

Proteinopathy-related neurophysiological changes and cognition

In terms of longitudinal cognitive changes evaluated by repeated administration of the Repeatable Battery for the Assessment of Neuropsychological Status (RBANS) neuropsychological assessment battery, we observed that individuals with high levels of both Aβ and tau showed more pronounced declines in the composite score calculated from the attention and immediate/delayed memory domains ($F_{(2, 93)} = 8.81$, $P_{FDR} = 0.001$; Fig. 4a). We then used linear models to test whether the interactive effects of continuous Aβ and tau SUVR values on neurophysiological activity were related to longitudinal cognitive performance (Fig. 2c). We found that individuals with a stronger moderating influence of tau deposition on the association of Aβ deposition with alpha-band activity have experienced a more pronounced cognitive decline, indicated by steeper negative slopes in the attention/memory composite score ($t_{(92)} = 3.37$, $P_{FDR} = 0.002$; Fig. 4b). When assessing each cognitive domain separately, we found the same interaction effect on the attention scores ($t_{(92)} = 3.58$, $P_{FDR} = 0.002$; Extended Data Table 2). Such associations remained significant after removing influential cases from each of the regression models, also extending to the immediate memory domain. The cognition analysis results were also replicated when using the temporal meta-ROI instead of the entorhinal cortex tau SUVR, both for the attention–memory composite score ($t_{(92)} = 2.48$, $P_{FDR} = 0.038$) and the attention scores ($t_{(92)} = 2.37$, $P_{FDR} = 0.038$). We did not find such associations with the Aβ–delta-band correlation values.

Predictive analysis of later-stage neurophysiological changes

Finally, we tested whether the magnitude of neurophysiological changes associated with the higher Aβ (whole brain) and tau (temporal meta-ROI) concentrations observed in later disease stages can be predicted from the interactive effects of Aβ and tau on alpha-band activity we observed in the preclinical data reported herein. To that end, we first retrieved the Aβ (cortical meta-ROI) and tau (temporal meta-ROI) deposition values reported in ref. 44, and the relative alpha-band power measurements reported in ref. 34 from independent but age-matched samples of participants presenting with MCI and probable AD. We used relative alpha-band power measures because our data showed this was the neurophysiological feature associated with longitudinal cognitive decline. We found that our model predictions overlapped substantially with these independent, empirical observations (Fig. 5). This analysis therefore supports the notion that the early synergistic interaction we observed between AD proteinopathies and neurophysiological activity in asymptomatic adults is consistent with and might be predictive of the related effects observed in the more advanced stages of the disease. We also emphasize this finding is robust against possible effects caused by different study sites, participant samples, PET tracers and MEG instruments.

Discussion

We report the first observations of interactive effects between early Aβ and tau pathology on cortical neurophysiological activity in asymptomatic adults with a family history of sporadic AD, and their associations with longitudinal cognitive decline. In line with predictions from in vivo and computational disease models, our data show that Aβ deposition

https://doi.org/10.1038/s41593-024-01763-8

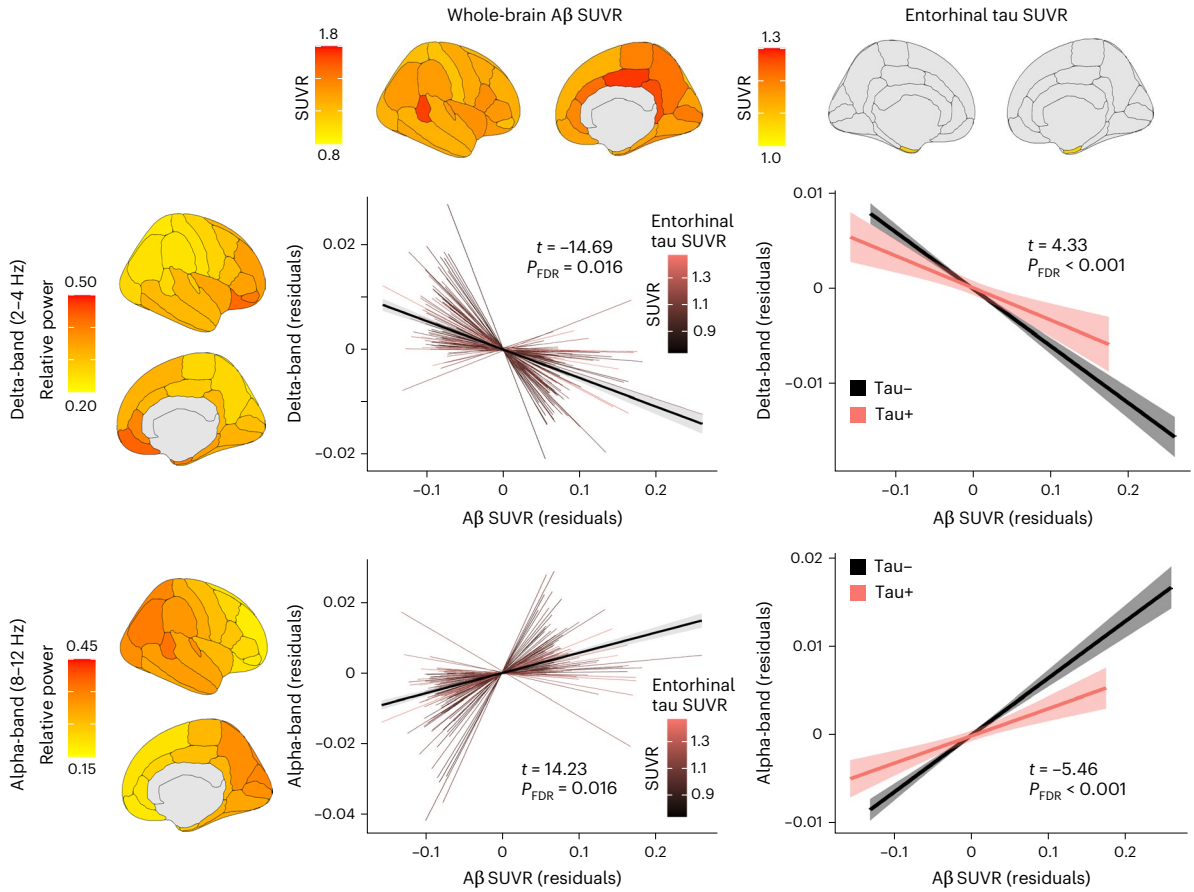

Fig. 3 | Interactive effects of AD proteinopathies on neurophysiological activity in asymptomatic adults. LME models show that Aβ was negatively associated with relative delta-band ($t_{(6967)} = -14.69$, $P_{FDR} = 0.016$) and positively associated with alpha-band ($t_{(6967)} = 14.23$, $P_{FDR} = 0.016$) power, suggesting an accelerating effect of Aβ on neurophysiological activity. Higher tau deposition in the entorhinal cortex was related to a shift towards neurophysiological slowing in these Aβ–neurophysiology associations (delta band–$t_{(6966)} = 4.33$, $P_{FDR} < 0.001$; alpha band–$t_{(6966)} = -5.46$, $P_{FDR} < 0.001$). Group average delta- and alpha-band relative power maps are shown on the left and average whole-brain Aβ and entorhinal SUVR maps are shown on top. Plots to the left indicate the nested relationship between Aβ and neurophysiological activity in the delta band (top) and alpha band (bottom), with lines of best fit for each participant indicated by thin colored lines representing entorhinal tau SUVR values and a thick black line representing the group main effect. Shaded region around the line of best fit across all participants represents the 95% confidence intervals. Plots to the right indicate the moderation of these nested Aβ–neurophysiological relationships by entorhinal tau deposition, with lines of best fit for individuals classified as tau-positive (red) and tau-negative (black), based on the group definition from the supplementary between-participant analysis. Shaded regions indicate 95% confidence intervals. Note that entorhinal tau SUVR values were treated as a continuous variable in all models and that the Tau−/Tau+ separation is only for visualization of the interaction effect. Corresponding *t* statistic and permuted, one-sided FDR corrected *P* values for the main effect of Aβ or the Aβ × Tau interaction are overlaid on each plot.

and neurophysiological enhancement of fast-frequency activity colocalize in the human cortex, before the emergence of clinical symptoms. We propose that when tau also starts to accumulate in the temporal lobe, the initial acceleration of neurophysiological activity related to Aβ deposition shifts towards neurophysiological slowing, accompanying cognitive decline. Although our interpretations are limited by the cross-sectional nature of our study, this body of results provides empirical evidence in humans for the hypothesized analogous hyperactive and hypoactive effects of Aβ and tau accumulation manifested as macroscopic spectral power changes in neurophysiological activity along the AD continuum, which has been suggested by decades of animal, late-stage human and computational modeling research. Our model estimates are also consistent with previously-reported levels of proteinopathy and neurophysiological changes observed later in the AD continuum (that is MCI and AD). As such, we anticipate that the present findings will inform more accurate models of AD progression and aid in the future identification of new prognostics and preventative targets.

Our study points at possible nonlinear interactions between AD proteinopathy and human cortical neurophysiology in asymptomatic individuals at risk of developing the disease. Our results are aligned with fMRI studies of prodromal AD[26,28,29] and confirm the predictions from recent computational models of preclinical AD[41]. We show that, as predicted from these models, early Aβ deposition is associated with expressions of neurophysiological enhancement of fast-frequency activity, as indexed by increased alpha-band and decreased delta-band activity[41,42]. Early tau deposition in medial–temporal regions can be hypothesized to synergistically trigger further pathological processes with Aβ[41,45], which our data suggest would manifest as a shift in neurophysiological activity. This shift occurs from a regime of accelerated oscillatory activity in the preclinical stage of the disease to a generalized slowing of activity in the subsequent prodromal and clinical stages of AD[31–34,39]. This effect was not present when using whole-brain tau measures, which emphasizes the pathological significance of early tau deposition in medial–temporal regions. However, our data also suggest that the shift in neurophysiological activity does affect the cortex broadly and beyond medio-temporal regions, as a possible precursor of the widespread slowing observed in the later phases of AD[39,40]. We found that this shift in neurophysiological dynamics is essentially driven by rhythmic brain activity, and not by broadband arrhythmic background activity.

https://doi.org/10.1038/s41593-024-01763-8

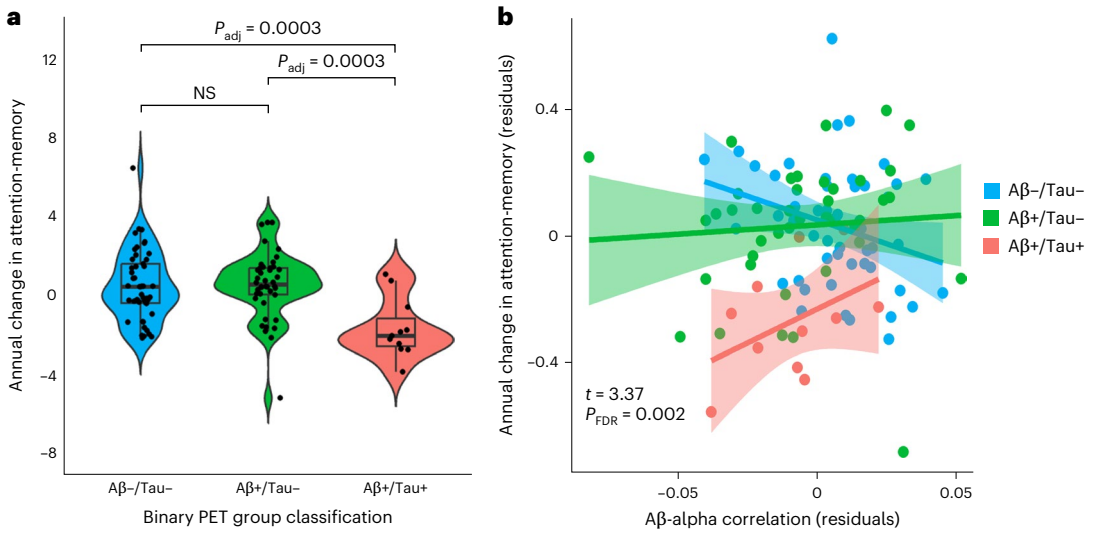

Fig. 4 | Neurophysiological impacts of AD proteinopathy are associated with longitudinal cognitive declines. a, Box plots show the median, quartiles, minima and maxima, while violin plots show the density distribution of the annual rate of change calculated for the RBANS attention–memory composite score (attention, immediate and delayed memory) of the participants, separated according to Aβ and tau positivity. The two-sided, one-factor ANCOVA analysis ($F_{(2, 93)} = 8.81$, $P_{FDR} = 0.001$) revealed that individuals expressing both Aβ and tau pathology (Aβ+/Tau+, $n = 11$) showed steeper cognitive decline compared to individuals with no pathology (Aβ−/Tau−, $n = 49$) and individuals with Aβ but no entorhinal cortex tau load (Aβ+/Tau−, $n = 42$). Tukey HSD P values adjusted for multiple comparisons are shown for the difference between the Aβ+/Tau+ and the Aβ−/Tau− and Aβ+/Tau− groups. **b**, Linear regression models demonstrated an interaction effect ($t_{(92)} = 3.37$, $P_{FDR} = 0.002$), where a more pronounced shift in the Aβ–alpha-band activity relationship for individuals with higher entorhinal tau was associated with longitudinal decline in attention–memory composite scores. The thick colored lines represent the line of best fit across participants in the Aβ−/Tau− (blue, $n = 49$), Aβ+/Tau− (green, $n = 42$) and Aβ+/Tau+ (red, $n = 11$) groups. The shaded area represents the 95% confidence intervals. Note that whole-brain Aβ and entorhinal tau SUVR values were treated as continuous variables for this analysis, and that participants were divided according to Aβ/Tau +/− groups only for visualization purposes. Corresponding t statistic and one-sided, FDR corrected P values are overlaid on the scatter plot.

Our study also provides direct evidence from human neurophysiology of analogous phenomena previously observed only in animal models of AD. Notably, our data support model predictions of how early, microscopic alterations at the neuronal circuit level also manifest as aberrant patterns at the macroscopic scale of neurophysiological activity. Computational models of AD pathophysiology predict that Aβ deposits induce toxic effects on the dynamics of neuronal circuits, by simultaneously increasing excitation and decreasing inhibition, leading to augmented levels of alpha-band activity[41]. According to these models, subsequent tau deposition damages axonal connections and reduces excitatory transmission, driving the neuronal dynamics towards a hypoactive regime, which manifests with decreased alpha-band activity at the macroscopic level. Our results support these predictions in human empirical data and are also in agreement with recent findings showing that macroscopic alterations of the neurophysiological frequency spectrum might be attributable to differential effects on the time constants of excitatory and inhibitory neuronal populations[46]. It is important to note that at least one modeling study has suggested that increased neuronal excitability in AD would instead be expressed as neurophysiological slowing at the macroscopic level[47]. Future experimental and computational modeling research elucidating the link between micro- and macroscopic expressions of aberrant neurophysiological activity is needed to fully contextualize our results.

Previous studies in patients with MCI and probable AD have reported that delta-band neurophysiological activity tracks disease progression along the AD continuum[33,34,42,48], and that the accumulation of Aβ[42] and postmortem tau pathology[32] are related to the magnitude of alpha-band activity, showing reduced alpha-band activity in later-stage AD[32,33,42]. Our results provide the first observations of this type in asymptomatic participants with a family history of AD, before they show cognitive symptoms. Notably, we demonstrate that in this group, there is a synergistic association of Aβ and tau pathologies with alpha-band neurophysiological activity, which is related to cognitive decline in attention and memory[32,33,42]. Reduced levels of alpha-band activity may precede subsequent increases in slower brain activity in the delta and theta bands, which are linked to impairments in additional cognitive domains, such as processing speed[34]. We further show that this model is also consistent with independent observations in the later stages of Aβ and tau pathology. These observations support the notion that early neurophysiological expressions of enhanced fast-frequency activity might presage the subsequent shift towards neurophysiological slowing and cognitive decline, as Aβ and tau continue to accumulate. However, the cross-sectional nature of our study limits our ability to draw definitive conclusions regarding the direction of these relationships. Future studies with longitudinal collection of neuroimaging data will further shed light on the temporality of AD pathological processes and changes in neurophysiological activity. We also look forward to future translational studies building on these new observations and proposed mechanisms, for new diagnostics, prognostics, outcome monitoring tools and ideally the definition of modifiable therapeutic targets. Our research agenda is to extend the present body of work towards the identification of robust neurophysiological and protein-pathological features to predict the possible progression to clinical AD, as well as to track the evolution of neurophysiological changes with the progressive accumulation of Aβ and tau, as we continue to follow the present cohort longitudinally.

We report synergistic associations between the early pathological deposition of Aβ and tau, and macroscopic neurophysiological activity in asymptomatic humans at risk of developing sporadic AD. By combining time-resolved MEG cortical mapping with Aβ and tau PET imaging, we demonstrate that Aβ depositions parallel an enhancement of fast-frequency neurophysiological activity in the asymptomatic human brain, and that tau deposition promotes a shift towards expressions of neurophysiological slowing related to longitudinal cognitive declines of attention and memory. These results support the long-standing

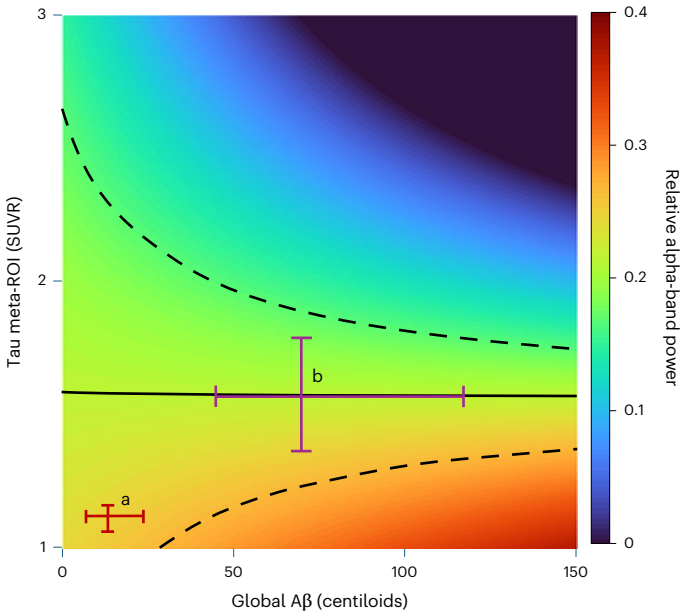

Fig. 5 | Independent validation of the synergistic association of proteinopathy with alpha-band neurophysiological activity in participants with MCI and early AD. We used the linear mixed-effects model coefficients of the interactive effect of Aβ and temporal meta-ROI tau on relative alpha-band power to infer the values of neurophysiological activity alpha-band power (colored heatmap) across increasing levels of global Aβ and temporal meta-ROI tau deposition along the AD continuum. The red cross (marked with 'a') represents the median and inter-quartile range of the empirical measures of global Aβ and temporal meta-ROI tau deposition of the present PREVENT-AD data in asymptomatic participants. The purple cross (marked with 'b') indicates the independent values reported in ref. 44 in MCI and probable AD participants. The black solid and dashed lines represent the median and inter-quartile range for the adjusted alpha-band power values independently reported in ref. 34. The heatmap shows that the model predictions from asymptomatic participant data are consistent with the empirical measures of global Aβ, temporal meta-ROI tau and alpha-band power reported in these two independent samples of participants with MCI and probable AD.

hypothesis that Aβ and tau differentially affect neural activity in the earliest stages of the AD continuum and provide foundations for future research on models and predictors of AD-related neurophysiology.

Online content

Any methods, additional references, Nature Portfolio reporting summaries, source data, extended data, supplementary information, acknowledgements, peer review information; details of author contributions and competing interests; and statements of data and code availability are available at https://doi.org/10.1038/s41593-024-01763-8.

References

1. Dubois, B. et al. Preclinical Alzheimer's disease: definition, natural history, and diagnostic criteria. *Alzheimers Dement.* **12**, 292–323 (2016).
2. Gale, S. A., Acar, D. & Daffner, K. R. Dementia. *Am. J. Med.* **131**, 1161–1169 (2018).
3. Jack, C. R. et al. Hypothetical model of dynamic biomarkers of the Alzheimer's pathological cascade. *Lancet Neurol.* **9**, 119–128 (2010).
4. Jack, C. R. et al. Revised criteria for diagnosis and staging of Alzheimer's disease: Alzheimer's Association Workgroup. *Alzheimers Dement.* **20**, 5143–5169 (2024).
5. Jagust, W. J. Imaging the evolution and pathophysiology of Alzheimer disease. *Nat. Rev. Neurosci.* **19**, 687–700 (2018).
6. Braak, H. & Braak, E. Staging of Alzheimer's disease-related neurofibrillary changes. *Neurobiol. Aging* **16**, 271–284 (1995).
7. Braak, H. & Braak, E. Neuropathological stageing of Alzheimer-related changes. *Acta Neuropathol.* **82**, 239–259 (1991).
8. Alzheimer, A. Über eine eigenartige erkrankung der hirnrinde. *Allg. Zschr. Psychiatr. Psych. Gerichtl. Med.* **64**, 146–148 (1907).
9. Sperling, R. A. et al. Toward defining the preclinical stages of Alzheimer's disease: recommendations from the National Institute on Aging–Alzheimer's Association workgroups on diagnostic guidelines for Alzheimer's disease. *Alzheimers Dement.* **7**, 280–292 (2011).
10. Palmqvist, S. et al. Earliest accumulation of β-amyloid occurs within the default-mode network and concurrently affects brain connectivity. *Nat. Commun.* **8**, 1214 (2017).
11. Villeneuve, S. et al. Existing Pittsburgh compound-B positron emission tomography thresholds are too high: statistical and pathological evaluation. *Brain* **138**, 2020–2033 (2015).
12. Mattsson, N., Palmqvist, S., Stomrud, E., Vogel, J. & Hansson, O. Staging β-amyloid pathology with amyloid positron emission tomography. *JAMA Neurol.* **76**, 1319–1329 (2019).
13. Thal, D. R., Rüb, U., Orantes, M. & Braak, H. Phases of Aβ-deposition in the human brain and its relevance for the development of AD. *Neurology* **58**, 1791–1800 (2002).
14. Leuzy, A. et al. Tau PET imaging in neurodegenerative tauopathies—still a challenge. *Mol. Psychiatry* **24**, 1112–1134 (2019).
15. Lowe, V. J. et al. Tau-positron emission tomography correlates with neuropathology findings. *Alzheimers Dement.* **16**, 561–571 (2020).
16. D'Amelio, M. & Rossini, P. M. Brain excitability and connectivity of neuronal assemblies in Alzheimer's disease: from animal models to human findings. *Prog. Neurobiol.* **99**, 42–60 (2012).
17. La Joie, R. et al. Prospective longitudinal atrophy in Alzheimer's disease correlates with the intensity and topography of baseline tau-PET. *Sci. Transl. Med.* **12**, 5732 (2020).
18. Selkoe, D. J. & Hardy, J. The amyloid hypothesis of Alzheimer's disease at 25 years. *EMBO Mol. Med.* **8**, 595–608 (2016).
19. Aschenbrenner, A. J., Gordon, B. A., Benzinger, T. L. S., Morris, J. C. & Hassenstab, J. J. Influence of tau PET, amyloid PET, and hippocampal volume on cognition in Alzheimer disease. *Neurology* **91**, e859–e866 (2018).
20. Busche, M. A. & Hyman, B. T. Synergy between amyloid-β and tau in Alzheimer's disease. *Nat. Neurosci.* **23**, 1183–1193 (2020).
21. Palop, J. J. & Mucke, L. Amyloid-β induced neuronal dysfunction in Alzheimer's disease: from synapses toward neural networks. *Nat. Neurosci.* **13**, 812–818 (2010).
22. Stargardt, A., Swaab, D. F. & Bossers, K. The storm before the quiet: neuronal hyperactivity and Aβ in the presymptomatic stages of Alzheimer's disease. *Neurobiol. Aging* **36**, 1–11 (2015).
23. Zott, B. et al. A vicious cycle of β amyloid-dependent neuronal hyperactivation. *Science* **365**, 559–565 (2019).
24. Busche, M. A. et al. Tau impairs neural circuits, dominating amyloid-β effects, in Alzheimer models in vivo. *Nat. Neurosci.* **22**, 57–64 (2019).
25. Palop, J. J. & Mucke, L. Network abnormalities and interneuron dysfunction in Alzheimer disease. *Nat. Rev. Neurosci.* **17**, 777–792 (2016).
26. Foster, C. M., Kennedy, K. M., Horn, M. M., Hoagey, D. A. & Rodrigue, K. M. Both hyper- and hypo-activation to cognitive challenge are associated with increased β-amyloid deposition in healthy aging: a nonlinear effect. *Neuroimage* **166**, 285–292 (2018).
27. Huijbers, W. et al. Amyloid-β deposition in mild cognitive impairment is associated with increased hippocampal activity, atrophy and clinical progression. *Brain* **138**, 1023–1035 (2015).
28. Leal, S. L., Landau, S. M., Bell, R. K. & Jagust, W. J. Hippocampal activation is associated with longitudinal amyloid accumulation and cognitive decline. *eLife* **6**, e22978 (2017).

29. Billette, O. V. et al. Novelty-related fMRI responses of precuneus and medial temporal regions in individuals at risk for Alzheimer disease. *Neurology* **99**, e775–e788 (2022).
30. Babiloni, C. et al. What electrophysiology tells us about Alzheimer's disease: a window into the synchronization and connectivity of brain neurons. *Neurobiol. Aging* **85**, 58–73 (2020).
31. López-Sanz, D., Bruña, R., de Frutos-Lucas, J. & Maestú, F. Magnetoencephalography applied to the study of Alzheimer's disease. *Prog. Mol. Biol. Transl. Sci.* **165**, 25–61 (2019).
32. Ranasinghe, K. G. et al. Reduced synchrony in α oscillations during life predicts post mortem neurofibrillary tangle density in early-onset and atypical Alzheimer's disease. *Alzheimers Dement.* **17**, 2009–2019 (2021).
33. Ranasinghe, K. G. et al. Neurophysiological signatures in Alzheimer's disease are distinctly associated with tau, amyloid-β accumulation, and cognitive decline. *Sci. Transl. Med.* **12**, eaaz4069 (2020).
34. Wiesman, A. I. et al. Spatio-spectral relationships between pathological neural dynamics and cognitive impairment along the Alzheimer's disease spectrum. *Alzheimers Dement. (Amst)* **13**, e12200 (2021).
35. De Haan, W. et al. Resting-state oscillatory brain dynamics in Alzheimer disease. *J. Clin. Neurophysiol.* **25**, 187–193 (2008).
36. Garcés, P. et al. Brain-wide slowing of spontaneous α rhythms in mild cognitive impairment. *Front. Aging Neurosci.* **5**, 100 (2013).
37. Poza, J., Hornero, R., Abásolo, D., Fernández, A. & Mayo, A. Evaluation of spectral ratio measures from spontaneous MEG recordings in patients with Alzheimer's disease. *Comput. Methods Programs Biomed.* **90**, 137–147 (2008).
38. López-Sanz, D., Serrano, N. & Maestú, F. The role of magnetoencephalography in the early stages of Alzheimer's disease. *Front. Neurosci.* **12**, 572 (2018).
39. Maestú, F. et al. The importance of the validation of M/EEG with current biomarkers in Alzheimer's disease. *Front. Hum. Neurosci.* **13**, 17 (2019).
40. Wiesman, A. I. et al. Spatially resolved neural slowing predicts impairment and amyloid burden in Alzheimer's disease. *Brain* **145**, 2177–2189 (2022).
41. Alexandersen, C. G., de Haan, W., Bick, C. & Goriely, A. A multi-scale model explains oscillatory slowing and neuronal hyperactivity in Alzheimer's disease. *J. R. Soc. Interface* **20**, 20220607 (2023).
42. Nakamura, A. et al. Electromagnetic signatures of the preclinical and prodromal stages of Alzheimer's disease. *Brain* **141**, 1470–1485 (2018).
43. Jack, C. R. et al. Defining imaging biomarker cut points for brain aging and Alzheimer's disease. *Alzheimers Dement.* **13**, 205–216 (2017).
44. Jack, C. R. et al. Predicting amyloid PET and tau PET stages with plasma biomarkers. *Brain* **146**, 2029–2044 (2023).
45. Lee, W. J. et al. Regional Aβ–tau interactions promote onset and acceleration of Alzheimer's disease tau spreading. *Neuron* **110**, 1932–1943 (2022).
46. Ranasinghe, K. G. et al. Altered excitatory and inhibitory neuronal subpopulation parameters are distinctly associated with tau and amyloid in Alzheimer's disease. *eLife* **11**, e77850 (2022).
47. Van Nifterick, A. M. et al. A multiscale brain network model links Alzheimer's disease-mediated neuronal hyperactivity to large-scale oscillatory slowing. *Alzheimers Res. Ther.* **14**, 101 (2022).
48. Gouw, A. A. et al. EEG spectral analysis as a putative early prognostic biomarker in nondemented, amyloid positive subjects. *Neurobiol. Aging* **57**, 133–142 (2017).

PREVENT-AD Research Group

Jonathan Gallego-Rudolf[1,2], Alexa Pichet Binette[1,3], Sylvia Villeneuve[1,2] & Sylvain Baillet[2]

Methods

Participants

The participants were from the PRe-symptomatic EValuation of Experimental or Novel Treatments for Alzheimer's Disease (PREVENT-AD) cohort[49], a large sample of asymptomatic middle-aged and older individuals with elevated familial risk of sporadic AD, defined as having one parent or multiple siblings affected by the disease[50,51]. As part of the inclusion criteria for the PREVENT-AD study, participants were required to (1) be at least 60 years of age or between 55 and 59 years if their age was 15 years younger than their first-affected relative's age at dementia onset, (2) have no history of major psychiatric or neurological disorders and (3) be rated as cognitively normal at the time of enrollment. Normal cognition at enrollment was determined by having a score ≥ 26 in the Montreal Cognitive Assessment[52] and a score of 0 in the Clinical Dementia Rating scale[53]. Normal cognition at the time of the MEG–PET sessions was determined by having a score ≥ 24 in the mini-mental state examination[54]. Participants whose scores exceeded the thresholds were further examined by a neuropsychologist from the PREVENT-AD group to verify their cognitive status. We retrieved data from a subsample of 124 PREVENT-AD participants, who all underwent Aβ and tau PET and resting-state MEG between 2017 and 2019 (ref. 49). No statistical methods were used to predetermine sample size, but our sample size is similar[55] or larger[34,42] to that reported in previous publications including multimodal imaging data (that is MEG, PET) in similar populations. From this subsample, the data from 20 participants were discarded, either due to issues with MEG data integrity (1 participant), PET data quality (1 participant) or unusable MEG data due to high-amplitude noise caused by ferromagnetic dental implants (18 participants). The final sample was therefore 104 participants (mean age = 67.4 years, s.d. = 4.9; 74 females; mean years of education = 15, s.d. = 3.1), who all provided informed consent that their de-identified data be used for research purposes reviewed and approved by the Institutional Review Board at McGill University, as the present study, with protocols compliant with the Declaration of Helsinki (protocol A05-B16-11B and A05-M55-11B). Participants received compensation to cover travel expenses and time. MEG data collection was performed blind to the Aβ/tau status of the participants. Data analysis was not performed blind to the conditions of the experiment, but group allocation was only implemented in the supplementary between-participants analysis.

Neuropsychological testing

The participants underwent yearly cognitive assessments using one of the four versions of the RBANS[56]. The RBANS is a practical neuropsychological tool to characterize abnormal cognitive decline in older adults. It yields scaled scores subdivided into five cognitive domains comprising immediate and delayed memory, attention, visuospatial constructional abilities and language. Longitudinal changes in cognition were assessed by estimating the linear slopes from the RBANS scores, computed using all available cognition timepoints obtained either before or after the MEG and PET visits (mean number of longitudinal cognitive assessments per participant = 6.6, s.d. = 2). We then normalized these slopes based on the average number of days between visits, and scaled the values to represent the annualized change in cognition. Considering that our participants were cognitively unimpaired at the time of the scans, and that the earliest cognitive impairments in AD are typically observed in the memory and attention domains[40,57,58], we averaged the estimated linear slopes from the attention and memory RBANS scores to derive a composite measure of cognitive decline. As a follow-up analysis, we also assessed each cognitive domain (attention, immediate and delayed memory) separately. To ensure that the effects reported are not biased by the variability of when the MEG visit occurred along this longitudinal trajectory, the relative temporal distance between the dates of the first cognitive assessment and the MEG visit (mean number of days = 1282.4, s.d. = 569.6) was included as a nuisance covariate in all statistical models involving longitudinal cognition.

Neuroimaging data acquisition and analysis

MRI. Structural MRIs were acquired at the Brain Imaging Center of the Douglas Research Centre (Montreal, Quebec, Canada) using a 3T Siemens TIM Trio Scanner equipped with a 12 or 32-channel coil (Siemens Medical Solutions). T1-weighted images were acquired using a MPRAGE sequence with the following parameters: 176 slices (1-mm slice thickness), repetition time = 2,300 ms, echo time = 2.98 ms, flip angle = 9°, FoV = 256 × 240 × 176 mm and voxel size = 1 mm^3. In the PREVENT-AD protocol, MRI data are collected annually as part of the longitudinal follow-up[51]. Here we used the structural scan acquired the closest to the MEG–PET visit (mean difference in days = 318.6, s.d. = 203.7).

We obtained the cortical surface from the T1-weighted structural MRI volumes of each individual using the FreeSurfer software package (version 5.3)[59]. We then parcellated the cortical surfaces according to the Desikan–Killiany atlas, comprising 34 × 2 bilateral cortical parcels[60]. This parcellation of individual cortical surfaces was used for MEG source mapping and SUVR quatification of the Aβ and tau PET data.

PET. PET imaging data were collected at the McConnell Brain Imaging Centre of the Montreal Neurological Institute and Hospital (Montreal, Quebec, Canada) using a Siemens HRRT head-only, high-resolution PET camera. Aβ scans were performed 40–70 min after injection of ~6 mCi of [18F] NAV4694 (Navidea Biopharmaceuticals), and tau scans were obtained 80–100 min after injection of ~10 mCi [18F] AV-1451 (FTP; Eli Lilly and Company). An attenuation scan was also acquired. Images were reconstructed using a 3D OP OSEM[61,62] (10 iterations, 16 subsets) algorithm, and were decay and motion corrected. Scatter correction was performed using a 3D scatter estimation method[62]. For most participants (n = 96), the two PET scans were acquired one day apart, and all but one were collected less than 5 months apart (mean = 6.9 days, s.d. = 29.3 days).

PET images were preprocessed using an in-house pipeline from the Villeneuve Lab (https://github.com/villeneuvelab/vlpp), as described in ref. 49. Briefly, the 4D image files (six frames of 5 min for NAV and four frames of 5 min for FTP) were realigned, averaged, and registered to their corresponding structural MRI. SUVR maps were generated by using the cerebellum gray matter as a reference region for Aβ scans, and the inferior cerebellum gray matter for tau scans. The PET signal was then averaged across each parcel from the Desikan–Killiany atlas. Considering the characteristics of our cohort, we report Aβ uptakes across the whole-brain and tau PET signal in the entorhinal cortex, because of evidence of early AD-related tau depositions in that region[6,7,43]. To account for the limitations of using a single small cortical region such as the entorhinal cortex for tau quantification, we repeated all analyses using an early tau-sensitive temporal meta-ROI (Extended Data Fig. 2), obtained by averaging SUVR values over the entorhinal cortex, fusiform gyrus, parahippocampal gyrus, lingual gyrus, and inferior and medial–temporal gyri[43]. Considering the high correlation between entorhinal and temporal meta-ROI tau SUVR values, we also repeated these analyses after excluding the entorhinal cortex from the temporal meta-ROI.

MEG. For most participants (n = 80) MEG was collected on the same day as one of the two PET visits using a 275-channel CTF system located inside a three-layer magnetically shielded room. The average time between MEG and PET data collection was 23 days for Aβ and 24.6 days for tau (s.d. = 57.4 and 60, respectively). Two 5-min runs (that is a total of 10 min) of resting state, eyes-open MEG data were collected from the participants, to derive robust measures of ongoing brain activity across the frequency spectrum[63]. We elected to use an eyes-open resting-state paradigm because, during eyes-open recordings, participants are less prone to experiencing drowsiness, which would confound the interpretation of neurophysiological slowing. Further, eye movements do occur behind the lids with the eyes closed, which are less stereotyped than eye blinks and therefore cause MEG artifacts

that are more challenging to correct. Participants were instructed to sit upright while looking at a fixation cross displayed on a screen. The data sampling rate was 2,400 Hz, with a hardware anti-aliasing low-pass filter set at 600 Hz. Built-in third-order gradient compensation was applied to attenuate environmental noise. We collected about 100 scalp points in each participant with a Polhemus Fastrak device, including anatomical landmarks at the nasion and the left and right preauricular points. We monitored head movements during MEG data collection with head position indicators attached to the participants' forehead and the left and right mastoids. We also collected reference signals for heartbeats and eye movements with concurrent electrocardiographic and electrooculographic recordings. Empty-room recordings (about 2 min) were obtained at the beginning of all MEG visits to characterize environmental noise at the time of each individual session.

We used Brainstorm3 for MEG data preprocessing and analysis[64,65] and followed recommended good-practice procedures[66]. The data were notch filtered to remove power-line noise and harmonics (60, 120, 180, 240 and 300 Hz), and high-pass filtered above 0.3 Hz to remove low-frequency drifts and MEG-sensor DC-offset. We inspected all MEG time series for bad channels and segments with prominent movement artifacts, which were marked and excluded from further analysis. Cardiac and eyeblink events were detected from their respective reference signals using an automated procedure[64]. We derived specific signal space projectors to attenuate eyeblink and heartbeat contaminants, and other stereotyped artifacts when necessary. We time segmented the MEG recordings into 4-s epochs, excluding segments that still contained major artifacts, as identified from the union of two standardized thresholds of ±3 median absolute deviations from the median—one for peak-to-peak signal amplitude and one for signal gradients.

MEG data were registered to individual structural T1-weighted scans using the scalp's digitized points. Using Brainstorm3, we obtained a MEG forward model (overlapping spheres) from 15,000 cortical locations for each participant. We estimated individualized sensor noise covariances from the empty-room recordings, which we then used to derive the participants' imaging kernels of depth-weighted dynamic statistical parametric mapping of cortical current flows oriented perpendicularly to the cortex[67]. We then derived the power spectrum density for each 4-s epoch of the cortical time series using Welch's estimator (2-s windows, 50% overlap). We then averaged all available epochs from both MEG runs to produce cortical maps of frequency band-specific activity in canonical frequency bands—delta (2–4 Hz), theta (5–7 Hz), alpha (8–12 Hz) and beta (15–29 Hz), each scaled relatively to the total power across all bands. Finally, we extracted the average relative signal power values in each frequency band of interest, and for each of the 68 cortical regions of the Desikan–Killiany atlas.

Statistics and reproducibility

Joint MEG–PET analysis. We first performed a between-participants analysis to test for potential whole-brain changes of neurophysiological (MEG) activity related to the pathological deposition of cortical Aβ and entorhinal tau. We derived the mean signal power across all cortical regions for each frequency band in the following three groups of participants: (1) participants with no Aβ nor entorhinal tau pathology (Aβ−/Tau−, $n = 50$), (2) participants with significant global Aβ burden but no entorhinal tau (Aβ+/Tau−, $n = 42$) and (3) participants with both global Aβ and entorhinal tau burden (Aβ+/Tau+, $n = 11$). The only participant (male) who was classified as Aβ−/Tau+ was excluded from the analysis. Aβ positivity was defined based on the average SUVR computed over a set of early Aβ sensitive regions (including the precuneus, posterior cingulate, parietal, frontal and lateral temporal cortices)[11]. Individuals with a global Aβ SUVR >1.18 (13.3 in Centiloid scale) were rated as Aβ+. This threshold was derived by estimating two s.d. above the mean global Aβ SUVR calculated from a normative subset of 11 young individuals who underwent the same PET protocol. Similarly, tau positivity was defined using a threshold of entorhinal SUVR >1.25, corresponding to two s.d. above the entorhinal SUVR values obtained for the young participants. We used the Levene test to assess variance homogeneity between our PET-defined groups, which showed that all of our models fulfilled this assumption (all $P > 0.05$). We ran an analysis of covariance (ANCOVA) to test whether the neurophysiological spectrum differed across groups while accounting for age, sex, years of education, hippocampal volume and the number of MEG epochs included as nuisance variables. We applied FDR corrections to account for the multiple (four) statistical tests performed across frequency bands. We then used bootstrapped resampling to derive confidence intervals around the mean statistics for each participant group while keeping the unbalanced proportion of individuals. To assess the robustness of these associations considering the small number of individuals within each group, we evaluated the presence of outliers by calculating the Cook's distance, a summary metric of how each observation influences the regression model. We repeated the analysis for each frequency band after removing the influential cases, defined as those having a Cook distance above three times the mean distance of all data points included in the model.

Considering that the residuals for some frequency bands (that is theta and alpha) were not normally distributed, and the issues around the imbalance in sample sizes between the PET subgroups defined in our between-participants analysis approach, we designed nested LME models to test the within-participants association between band-specific neurophysiological activity and PET markers of AD pathology, accounting for potential confounds of age, sex, years of education, hippocampal volume and number of MEG epochs included per participant. Specifically, we tested for consistent within-participant relationships between Aβ deposition and neurophysiological activity across all cortical regions (neurophys. ~Aβ + age + sex + education + hippocampal volume + number of MEG epochs, random = ~1|participant), as well as the interactive effect of entorhinal tau deposition on these relationships across individuals (neurophys. ~Aβ × Tau + age + sex + education + hippocampal volume + number of MEG epochs, random = ~1 | participant). Both Aβ and entorhinal tau were treated as continuous variables for this analysis. We repeated our Aβ × Tau models by using the temporal meta-ROI instead of the entorhinal cortex tau SUVR values, and also by incorporating whole-brain estimates of tau deposition across all cortical regions as a nested variable of interest (neurophys. ~Aβ × regional Tau + age + sex + education + hippocampal volume + number of MEG epochs, random = ~1 | participant).

To visualize the synergistic interaction of tau deposition with the Aβ-neurophysiology relationships, we plotted the association between Aβ and neurophysiological activity separately for participants in the Tau+ and Tau− groups, based on the threshold defined for the between-participant analysis. For the models that included whole-brain regional tau as a nested variable, we showed the interaction effect by plotting the line of best fit obtained by separating the cortical regions exhibiting the highest and lowest (that is upper and lower quartiles) levels of tau within each participant. To ensure robustness, we performed 1,000 nonparametric permutations by randomly shuffling the Aβ SUVR values across the 68 cortical regions of each individual while keeping the MEG maps and all other covariates intact. For the models including whole-brain tau as a nested variable, we ran the permutations by shuffling between pairs of Aβ and tau estimates to preserve any interactive association between data points. From these permuted models, we then built a null distribution of the t statistic obtained for the relevant main effect (that is Aβ) or the interaction of Aβ × Tau and calculated the probability (P value) of obtaining the comparable statistic from the original model. We implemented FDR corrections to adjust the permuted P values accounting for the multiple statistical comparisons across the four frequency bands of interest. To test whether these relationships were confounded by global spectral changes of aperiodic neurophysiological activity, we repeated all analyses with LME models that included the region-wise aperiodic slope and offset of the neurophysiological power spectrum as a nuisance covariate[68,69].

We parameterized the power spectrum data obtained at each atlas region by using the specparam module in Brainstorm3 (Matlab, version R2021b) using the recommended default parameters[69]—frequency range 1–40 Hz, Gaussian peak model with peak width limits between 0.5 and 12 Hz, and a maximum number of three detectable peaks, a minimum peak height of 0.3 dB and a proximity threshold equivalent to two s.d. from the largest peak, with a fixed aperiodic and no guess weight. As mentioned above, we also repeated all LME analyses using the tau SUVR values from the temporal meta-ROI instead of those from the entorhinal cortex and the nested tau estimates across all cortical regions. All statistical analyses were computed using R (version 4.1.1)[70]. LME models were computed using the nlme package (version 3.1.152)[71], ggplot2 (version 3.4.0)[72] and ggseg (version 1.6.5)[73] for visualization.

Association with cognitive decline. We first assessed whether longitudinal cognition differed across Aβ−/Tau−, Aβ+/Tau− and Aβ+/Tau+ individuals, by running an ANCOVA and posthoc Tukey's Honestly Significant Differences (HSD) tests. We then tested whether the strength of any significant relationship between neurophysiological activity and AD proteinopathy was associated with longitudinal changes in cognitive performance. For each participant, we calculated the Fisher-transformed (atanh function in R) Pearson correlation coefficient between Aβ concentrations and neurophysiological signal power across all cortical regions. We restricted the analysis to the alpha and delta frequency bands because they showed significant associations with AD pathology. We fitted a linear model in R between the longitudinal cognitive scores described in neuropsychological testing above and the continuous Aβ–neurophysiology correlation coefficients, with tau concentrations as a moderating factor (lm function; cognitive slope ~(Aβ-neurophys. correlation) × Tau + age + sex + education + hippocampal volume + number of MEG epochs + time between MEG and the first cognition timepoint). We performed these analyses with 102 individuals, after excluding the Aβ−/Tau+ participant and the participant (female) who had completed only one cognitive assessment. We then applied FDR corrections to account for the four statistical comparisons across the composite attention–memory scores and the individual cognitive domains. Once again, we identified influential cases for each regression model using Cook's distance approach described above and recomputed the analyses after removing individuals identified as potential outliers.

Predicting neurophysiological changes in later disease stages. Finally, we tested whether our linear mixed-effects model estimates matched the levels of neurophysiological changes reported in later disease stages. We used the coefficients from our linear mixed-effect model relating region-wise Aβ, temporal meta-ROI tau deposition and relative alpha-band power to estimate whole-brain relative alpha-band power values across a wider range of increasing levels of Aβ and tau deposition while keeping all other covariates constant (by multiplying their model coefficients by the median values calculated across all participants). To facilitate direct comparison with other studies, we expressed our global Aβ deposition estimates in Centiloid units for visualization, which was achieved by converting our NAV4694 SUVR values following the procedures described in ref. 74 to validate and adapt the NAV4694 SUVR to Centiloid formula proposed in ref. 75. We then compared these estimates against the median global Aβ, temporal meta-ROI tau SUVR and whole-brain relative alpha-band power values reported in two independent studies of participants with MCI and AD[34,44]. The participant samples were similar to our cohort in terms of age (PREVENT-AD—median = 66.3, IQR = 64.2, 70.6; ref. 44—median = 72.7, IQR = 65.8, 80.1; ref. 34—median = 70, IQR = 64, 74). For Aβ and tau, we used the estimates reported in ref. 44, calculated across 272 cognitively impaired patients. We calculated the weighted mean of the global Aβ Centiloid and tau meta-ROI flortaucipir SUVR values reported for the MCI and AD groups used in this work. For the relative alpha-band power estimates, we used the median and quartiles from 38 MCI and mild probable AD patients reported in ref. 34. Because these measures were from eyes-closed resting-state data, and our data were collected with eyes-open, we adjusted the values from ref. 34 with the multiplicative eyes-open to eyes-closed ratio reported in ref. 76 (median = 0.21, IQR = 0.16, 0.26). We then overlayed the median and quartile estimates of Aβ and tau from ref. 44 and the adjusted relative alpha-band power from ref. 34 on top of a heatmap produced from our model estimates (Fig. 5). We also verified that the alignment between the three independent datasets was similar when using a more conservative eyes-open to eyes-closed correction ratio[77] (median = 0.16, IQR = 0.11, 0.21) and when using no correction (median = 0.24, IQR = 0.19, 0.29).

Reporting summary

Further information on research design is available in the Nature Portfolio Reporting Summary linked to this article.

Data availability

Data used in the preparation of this manuscript were obtained from the Presymptomatic Evaluation of Experimental or Novel Treatments for Alzheimer's Disease (PREVENT-AD, https://prevent-alzheimer.net/). Some of the data are publicly available (https://openpreventad.loris.ca/, and https://www.mcgill.ca/bic/neuroinformatics/omega). In compliance with the ethical and privacy policies stipulated in the PREVENT-AD study to protect the identity of the participants and to preserve their right to refrain from sharing part of their biological/imaging data openly, the full internal release of the dataset https://registeredpreventad.loris.ca/ can only be shared upon approval by the scientific committee at the Centre for Studies on Prevention of Alzheimer's Disease (StoP-AD) at the Douglas Research Centre. Detailed instructions for accessing the open and requesting access to the full internal release versions of the PREVENT-AD dataset can be found at https://prevent-alzheimer.net/?page_id=1760&lang=en. For more details regarding the organization of the PREVENT-AD dataset, please refer to refs. 50,51. For further about getting access to the PREVENT-AD dataset please contact co-author S. Villeneuve (sylvia.villeneuve@mcgill.ca). The Desikan–Killiany atlas parcellation is included in FreeSurfer version 5.3 (https://surfer.nmr.mgh.harvard.edu/fswiki/CorticalParcellation) and the ggseg package version 1.6.5 (https://github.com/ggseg). Centiloid data transformation was done by adapting a formula for our NAV4694 tracer following the steps described in refs. 74,75. The normative NAV4694 data necessary for the Centiloid validation can be found on the GAAIN website of the Alzheimer Association (https://www.gaain.org/centiloid-project).

Code availability

MRI parcellation was done using the FreeSurfer software (version 5.3). PET analysis was performed using a standard pipeline available at https://github.com/villeneuvelab/vlpp. The 3D OSEM algorithm has been described in previous publications[61,62]. MEG data analysis was implemented using the Brainstorm software package (Brainstorm3) working in Matlab (version 2021b). All the statistical analyses reported in this manuscript were conducted using documented functions from the openly distributed R software (version 4.1.1). Linear mixed-effects models were implemented using nlme (version 3.1.152). Data plots were generated using ggplot2 (version 3.4.0) and brain plots using ggseg (version 1.6.5). The scripts generated to implement the statistical analyses presented in this manuscript are hosted in an open-access GitHub repository, available at https://github.com/jogaru1818/AD_proteinopathy_neurophysiology.

References

49. McSweeney, M. et al. Intermediate flortaucipir uptake is associated with Aβ-PET and CSF tau in asymptomatic adults. *Neurology* **94**, e1190–e1200 (2020).

50. Breitner, J. C. S., Poirier, J., Etienne, P. E. & Leoutsakos, J. M. Rationale and structure for a new center for Studies on Prevention of Alzheimer's Disease (StoP-AD). *J. Prev. Alzheimers Dis.* **3**, 236–242 (2016).
51. Tremblay-Mercier, J. et al. Open science datasets from PREVENT-AD, a longitudinal cohort of pre-symptomatic Alzheimer's disease. *Neuroimage Clin.* **31**, 102733 (2021).
52. Nasreddine, Z. S. et al. The Montreal Cognitive Assessment, MoCA: a brief screening tool for mild cognitive impairment. *J. Am. Geriatr. Soc.* **53**, 695–699 (2005).
53. Hughes, C. P., Berg, L., Danziger, W. L., Coben, L. A. & Martin, R. L. A new clinical scale for the staging of dementia. *Br. J. Psychiatry* **140**, 566–572 (1982).
54. Folstein, M. F., Folstein, S. E. & Mchugh, P. R. 'Mini-mental state'. A practical method for grading the cognitive state of patients for the clinician. *J. Psychiatr. Res.* **12**, 189–198 (1975).
55. López-Sanz, D. et al. Alpha band disruption in the AD-continuum starts in the subjective cognitive decline stage: a MEG study. *Sci. Rep.* **6**, 37685–37695 (2016).
56. Randolph, C., Tierney, M. C., Mohr, E. & Chase, T. N. The Repeatable Battery for the Assessment of Neuropsychological Status (RBANS): preliminary clinical validity. *J. Clin. Exp. Neuropsychol.* **20**, 310–319 (1998).
57. Malhotra, P. A. Impairments of attention in Alzheimer's disease. *Curr. Opin. Psychol.* **29**, 41–48 (2019).
58. Jahn, H. Memory loss in Alzheimer's disease. *Dialogues Clin. Neurosci.* **15**, 445–454 (2013).
59. Fischl, B. FreeSurfer. *Neuroimage* **62**, 774–781 (2012).
60. Desikan, R. S. et al. An automated labeling system for subdividing the human cerebral cortex on MRI scans into gyral based regions of interest. *Neuroimage* **31**, 968–980 (2006).
61. Varrone, A. et al. Advancement in PET quantification using 3D-OP-OSEM point spread function reconstruction with the HRRT. *Eur. J. Nucl. Med. Mol. Imaging* **36**, 1639–1650 (2009).
62. Sibomana, M., Keller, S. H., Stute, S. & Comtat, C. Benefits of 3D scatter correction for the HRRT—a large axial FOV PET scanner. *Proceedings of the 2012 IEEE Nuclear Science Symposium and Medical Imaging Conference Record (NSS/MIC)*, 2954–2957 (IEEE, 2012).
63. Wiesman, A. I., da Silva Castanheira, J. & Baillet, S. Stability of spectral estimates in resting-state magnetoencephalography: recommendations for minimal data duration with neuroanatomical specificity. *Neuroimage* **247**, 118823 (2022).
64. Niso, G. et al. Brainstorm pipeline analysis of resting-state data from the open MEG archive. *Front. Neurosci.* **13**, 284 (2019).
65. Tadel, F., Baillet, S., Mosher, J. C., Pantazis, D. & Leahy, R. M. Brainstorm: a user-friendly application for MEG/EEG analysis. *Comput. Intell. Neurosci.* **2011**, 879716 (2011).
66. Gross, J. et al. Good practice for conducting and reporting MEG research. *Neuroimage* **65**, 349–363 (2013).
67. Baillet, S. Magnetoencephalography for brain electrophysiology and imaging. *Nat. Neurosci.* **20**, 327–339 (2017).
68. Wilson, L. E., da Silva Castanheira, J. & Baillet, S. Time-resolved parameterization of aperiodic and periodic brain activity. *eLife* **11**, e77348 (2022).
69. Donoghue, T. et al. Parameterizing neural power spectra into periodic and aperiodic components. *Nat. Neurosci.* **23**, 1655–1665 (2020).
70. R Core Team. *R: A Language and Environment for Statistical Computing* (R Foundation for Statistical Computing, 2021).
71. Pinheiro, J. & Bates, D. nlme: linear and nonlinear mixed effects models cran.r-project.org/web/packages/nlme/index.html (2022).
72. Wickham, H. *Ggplot2: Elegant Graphics for Data Analysis* (Springer-Verlag, 2016).
73. Mowinckel, A. M. & Vidal-Piñeiro, D. Visualization of brain statistics with R packages ggseg and ggseg3d. *Adv. Methods Pract. Psychol. Sci.* **3**, 466–483 (2020).
74. Klunk, W. E. et al. The Centiloid project: standardizing quantitative amyloid plaque estimation by PET. *Alzheimers Dement.* **11**, 1–15 (2015).
75. Rowe, C. C. et al. Standardized expression of 18F-NAV4694 and 11C-PiB β-amyloid PET results with the Centiloid scale. *J. Nucl. Med.* **57**, 1233–1237 (2016).
76. Anwar, A. R. et al. Multi-modal causality analysis of eyes-open and eyes-closed data from simultaneously recorded EEG and MEG. *Proceedings of the 36th Annual International Conference of the IEEE Engineering in Medicine and Biology Society* 2825–2828 (IEEE, 2014).
77. Hata, M. et al. Alpha event-related synchronization after eye closing differs in Alzheimer's disease and dementia with Lewy bodies: a magnetoencephalography study. *Psychogeriatrics* **18**, 202–208 (2018).

Acknowledgements

The authors acknowledge all the PREVENT-AD participants and their families, the PREVENT-AD team members, as well as the Brain Imaging Center of the Douglas Research Centre and the PET and cyclotron units of the Montreal Neurological Institute for their time and dedication to this project. A complete list of PREVENT-AD contributors can be found at https://preventad.loris.ca/acknowledgements/acknowledgements.php?date=2024-06-26. The investigators of the PREVENT-AD program contributed to the design and implementation of PREVENT-AD and/or provided data but did not participate in analyzing or writing of this report. The authors would also like to thank the reviewers for providing their valuable insight, and V. Ourry, F. St-Onge, Y. Yakoub, M. Javanray, T. Qiu, J. Remz, A. Fajardo-Valdez and J. da Silva Castanheira for providing advice on the study research design. This project has been made possible by the Canada Brain Research Fund (CBRF), an innovative arrangement between the Government of Canada (through Health Canada) and Brain Canada Foundation, and the Alzheimer's Association, via a grant to S.B. J.G.R. is supported by the Mexican National Council of Science and Technology (CONACyT; 2020-000017-02EXTF-00402) and the Healthy Brains Healthy Lives (HBHL) program at McGill University. A.I.W. is supported by grant F32-NS119375 from the United States National Institutes of Health and a Banting Postdoctoral Fellowship (BPF-186555) from the Canadian Institutes of Health Research. S.V. is supported by the Alzheimer Society of Canada, the Alzheimer Association and the Canadian Institutes of Health Research (CIHR; 438655). S.B. is supported by the United States National Institutes of Health (NIH; R01-EB026299-05), the Tier-1 Canadian Institutes of Health Research Canada Research Chair of Neural Dynamics of Brain Systems (CRC-2017-00311) and a Discovery Grant from the Natural Sciences and Engineering Research Council of Canada (436355-13). The PREVENT-AD Research Group receives funding from the J.L. Levesque Foundation, Brain Canada and the Fonds de Recherche du Québec—Sante (FRQS).

Author contributions

J.G.R., A.I.W., S.V. and S.B. conceptualized the study, and reviewed, edited and wrote the manuscript. J.G.R., A.I.W., A.P.B., S.V. and S.B. were responsible for methodology. J.G.R., A.I.W. and A.P.B. handled software development and conducted formal analysis. J.G.R. and A.I.W. validated the data. J.G.R., A.P.B., S.V. and S.B. performed data curation. J.G.R. helped in study visualization. J.G.R., S.V. and S.B. led the investigation. S.V. and S.B. contributed to resources, supervision, project administration, and funding acquisition. J.G.R., A.P.B., S.V. and S.B. are contributors to the PREVENT-AD Research Group.

Competing interests
The authors declare no competing interests.

Additional information
Extended data is available for this paper at https://doi.org/10.1038/s41593-024-01763-8.

Supplementary information The online version contains supplementary material available at https://doi.org/10.1038/s41593-024-01763-8.

Correspondence and requests for materials should be addressed to Sylvain Baillet.

Peer review information *Nature Neuroscience* thanks Willem de Haan, Masud Husain and the other, anonymous, reviewer(s) for their contribution to the peer review of this work.

https://doi.org/10.1038/s41593-024-01763-8

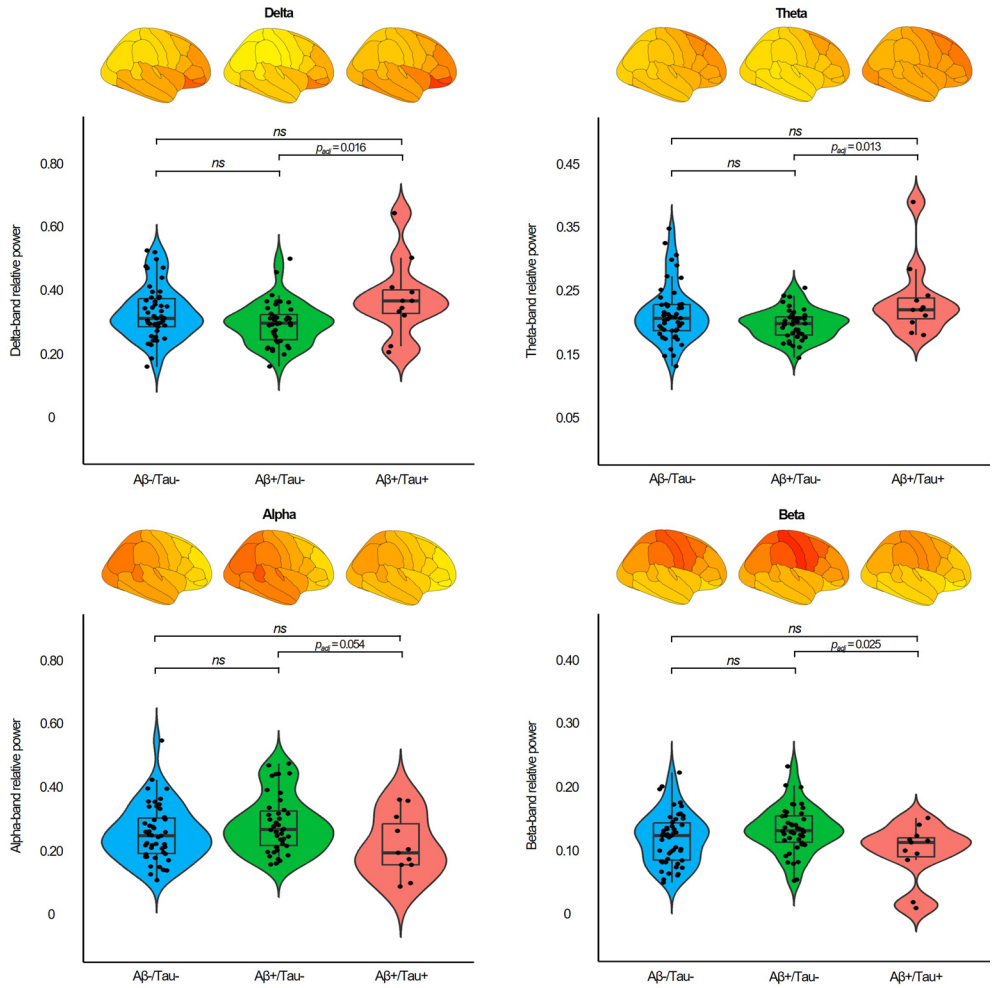

Extended Data Fig. 1 | Between-subjects spectral power analysis. Box plots show the median, quartiles, minima and maxima, while violin plots show the density distribution of the mean whole-brain relative spectral power values for the delta, theta, alpha and beta frequency bands across subjects with no AD pathology (Aβ−/Tau−, $n = 50$), subjects with widespread Aβ expression and low entorhinal tau (Aβ+/Tau−, $n = 42$) and subjects with both Aβ and entorhinal tau burden (Aβ+/Tau+, $n = 11$). Mean relative power brain maps for each subgroup are shown on top of each plot. Two-sided, one-factor ANCOVAs were performed to assess the main effect of group on whole-brain relative power. A neurophysiological slowing effect was observed for the Aβ+/Tau+ compared to the Aβ+/Tau− group, reflected as an increase in whole-brain delta ($F_{(2, 95)} = 4.58$, $p_{FDR} = 0.025$) and theta ($F_{(2, 95)} = 4.76$, $p_{FDR} = 0.025$) power and a decrease in alpha ($F_{(2, 95)} = 3.15$, $p_{FDR} = 0.047$) and beta ($F_{(2, 95)} = 3.79$, $p_{FDR} = 0.034$) power. Brackets indicate the results from post hoc comparisons to assess significant differences between the groups, with their corresponding Tukey HSD p-values adjusted for multiple comparisons. *ns*: non-significant.

https://doi.org/10.1038/s41593-024-01763-8

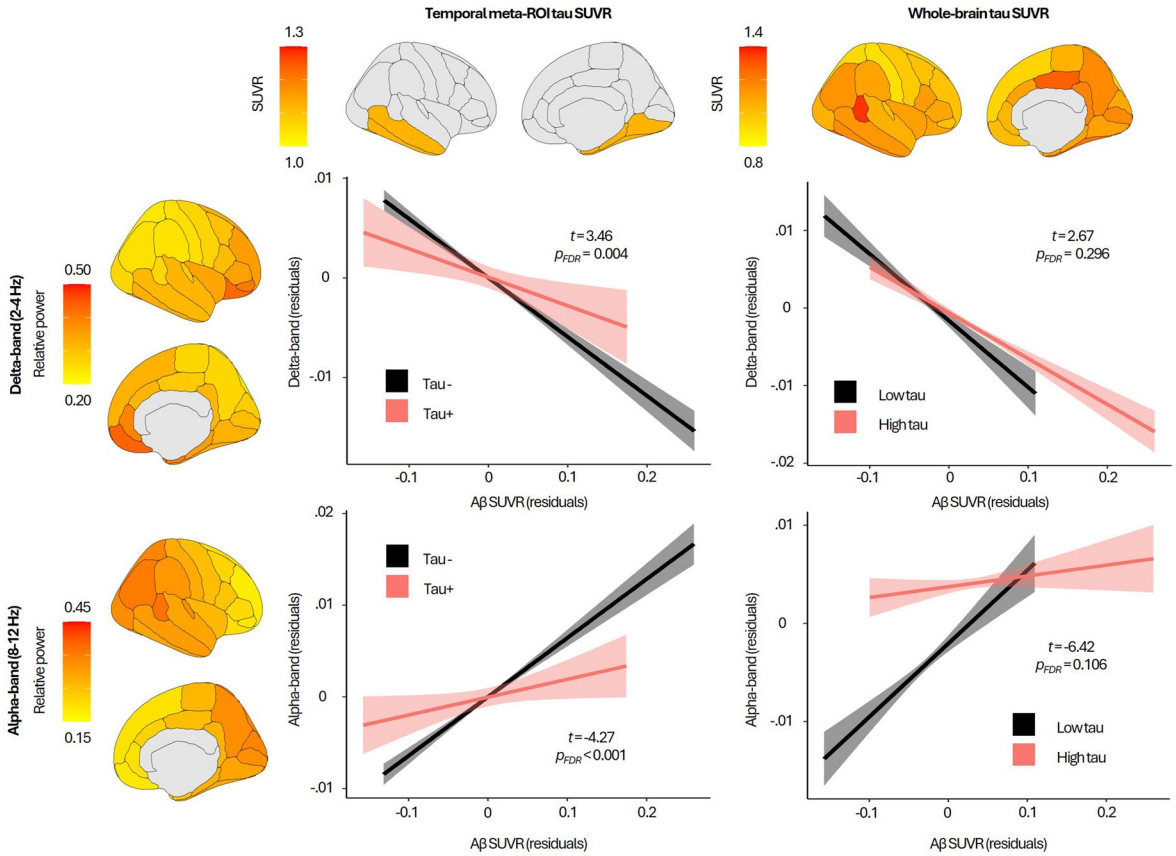

Extended Data Fig. 2 | Interactive Aβ and tau effect on neurophysiological activity using temporal meta-ROI and whole-brain regional tau. The observation that higher tau deposition relates to a shift in the Aβ-neurophysiology associations was replicated when using the average temporal meta-ROI instead of the entorhinal cortex tau SUVR values (alpha: $t_{(6966)} = -4.27$, $p_{FDR} < 0.001$; delta: $t_{(6966)} = 3.46$, $p_{FDR} = 0.004$; left panel). The thick colored lines represent the line-of-best fit across the Tau− (black; $n = 11$) and Tau+ (red; $n = 93$) participants. The shaded area represents the 95% confidence intervals. The same trend was observed when using nested, whole-brain regional tau SUVR values, although the associations were not significant after permutation and FDR corrections (alpha-band: $t_{(6965)} = -6.42$, $p_{FDR} = 0.106$; delta-band: $t_{(6965)} = 2.67$, $p_{FDR} = 0.296$; right panel). The thick colored lines represent the line-of-best fit across the bottom quartile low tau (black) and the top quartile high tau (red) regions. The shaded area represents the 95% confidence intervals. Group average delta- and alpha-band relative power maps are shown on the left and average temporal meta-ROI and whole-brain tau SUVR maps are shown on top. Note that tau SUVR values were treated as a continuous variable in all analyses, and that the Tau−/Tau+ and low/high tau distinctions were used only for visualization of the interaction effects. Corresponding t statistic and permuted, one-sided FDR corrected p-values are overlaid on each plot. Shaded regions indicate 95% confidence intervals.

https://doi.org/10.1038/s41593-024-01763-8

Extended Data Table 1 | Replication of whole-brain averaged between-participants spectral power analysis after removing influential cases

Between-subjects spectral power analysis								
MEG frequency band	Aβ-/Tau- mean (CI)	Aβ+/Tau- mean (CI)	Aβ+/Tau+ mean (CI)	ANCOVA *F* statistic	*p*-value	Aβ-/Tau- vs Aβ+/Tau-	Aβ-/Tau- vs Aβ+/Tau+	Aβ+/Tau- vs Aβ+/Tau+
Delta-band (2-4 Hz)	0.33 (0.30-0.35)	0.29 (0.27-0.31)	0.37 (0.34-0.42)	6.59 (2,90)	**0.008**	**0.026**	0.191	**0.005**
Theta-band (5-7 Hz)	0.20 (0.19-0.21)	0.19 (0.18-0.20)	0.21 (0.20-0.22)	2.75 (2,85)	0.069	0.176	0.603	0.127
Alpha-band (8-12 Hz)	0.24 (0.22-0.27)	0.27 (0.25-0.30)	0.20 (0.15-0.25)	4.38 (2,90)	**0.030**	0.177	0.188	**0.016**
Beta-band (15-29 Hz)	0.11 (0.10-0.12)	0.13 (0.12-0.14)	0.11 (0.10-0.12)	2.79 (2,85)	0.069	0.098	0.850	**0.016**

Summary of the between-participants analysis comparing whole-brain averaged neurophysiological activity spectral power across PET-defined subgroups after removing influential cases. As presented in Table 2, we indicate each group's mean and confidence intervals of the relative power for each frequency band, followed by statistics from the two-sided, one-factor ANCOVA test (*F* statistic (df) and FDR corrected *p*-values) and post hoc pairwise comparisons (Tukey HSD corrected *p*-values). Significant differences between the groups (corrected $p < 0.05$) are highlighted in bold. The increased delta and reduced alpha power effects observed in the Aβ+/Tau+ compared to the Aβ+/Tau− individuals remained statistically significant after removing influential observations.

https://doi.org/10.1038/s41593-024-01763-8

Extended Data Table 2 | Interactive effects of neurophysiological changes in Alzheimer's disease proteinopathy on cognition

Cognition ~ [Ab-Neurophys. Corr] * Tau entorhinal				
	Full sample		Without outliers	
Cognitive domain	*t* statistic	*p*-value	*t* statistic	*p*-value
Attention	3.58 (92)	**0.002**	3.61 (84)	**0.001**
Immediate memory	1.55 (92)	0.164	3.21 (82)	**0.001**
Delayed memory	0.98 (92)	0.327	1.47 (85)	0.142
Attention / memory score	3.37 (92)	**0.002**	4.35 (87)	**< 0.001**

Summary of the statistical analyses addressing the effect of a more pronounced shift in the Aβ-alpha activity relationship for individuals with higher entorhinal tau and longitudinal cognitive declines across attention and memory domains. The table shows the obtained *t* statistic (df) and FDR corrected *p*-values for the composite attention/memory score and for each cognitive domain, evaluated separately. Significant differences between the groups (corrected $p<0.05$) are highlighted in bold. A significant interaction effect was observed for the attention/memory composite score and individually for the attention domain. Removing influential cases from each regression model produced the same results, with the addition of a significant interaction effect for the immediate memory domain.

nature portfolio

Corresponding author(s): Sylvain Baillet

Last updated by author(s): Jul 5, 2024

Reporting Summary

Nature Portfolio wishes to improve the reproducibility of the work that we publish. This form provides structure for consistency and transparency in reporting. For further information on Nature Portfolio policies, see our Editorial Policies and the Editorial Policy Checklist.

Statistics

For all statistical analyses, confirm that the following items are present in the figure legend, table legend, main text, or Methods section.

n/a	Confirmed
☐	☒ The exact sample size (*n*) for each experimental group/condition, given as a discrete number and unit of measurement
☐	☒ A statement on whether measurements were taken from distinct samples or whether the same sample was measured repeatedly
☐	☒ The statistical test(s) used AND whether they are one- or two-sided *Only common tests should be described solely by name; describe more complex techniques in the Methods section.*
☐	☒ A description of all covariates tested
☐	☒ A description of any assumptions or corrections, such as tests of normality and adjustment for multiple comparisons
☐	☒ A full description of the statistical parameters including central tendency (e.g. means) or other basic estimates (e.g. regression coefficient) AND variation (e.g. standard deviation) or associated estimates of uncertainty (e.g. confidence intervals)
☐	☒ For null hypothesis testing, the test statistic (e.g. *F*, *t*, *r*) with confidence intervals, effect sizes, degrees of freedom and *P* value noted *Give P values as exact values whenever suitable.*
☒	☐ For Bayesian analysis, information on the choice of priors and Markov chain Monte Carlo settings
☐	☒ For hierarchical and complex designs, identification of the appropriate level for tests and full reporting of outcomes
☐	☒ Estimates of effect sizes (e.g. Cohen's *d*, Pearson's *r*), indicating how they were calculated

Our web collection on statistics for biologists contains articles on many of the points above.

Software and code

Policy information about availability of computer code

Data collection	No specialized commercial software were used for data collection
Data analysis	MRI parcellation was done using the FreeSurfer software (version 5.3). PET analysis was performed using a standard pipeline available in https://github.com/villeneuvelab/vlpp. The 3D OSEM algorithm has been described in previous publications. MEG data analysis was implemented using the Brainstorm software package (Brainstorm3) working in Matlab (version 2021b). All the statistical analysis reported in this manuscript were conducted using documented functions from the openly distributed R software (version 4.1.1). Linear Mixed Effects models were implemented using nlme (version 3.1.152). Data plots were generated using ggplot2 (version 3.4.0) and brain plots using ggseg (version 1.6.5). The scripts generated to implement the statistical analyses presented in this manuscript are hosted in an open-access GitHub repository, available in https://github.com/jogaru1818/AD_proteinopathy_neurophysiology.

For manuscripts utilizing custom algorithms or software that are central to the research but not yet described in published literature, software must be made available to editors and reviewers. We strongly encourage code deposition in a community repository (e.g. GitHub). See the Nature Portfolio guidelines for submitting code & software for further information.

Data

Policy information about availability of data

All manuscripts must include a data availability statement. This statement should provide the following information, where applicable:

- Accession codes, unique identifiers, or web links for publicly available datasets
- A description of any restrictions on data availability
- For clinical datasets or third party data, please ensure that the statement adheres to our policy

Data used in the preparation of this manuscript were obtained from the Pre-symptomatic Evaluation of Experimental or Novel Treatments for Alzheimer's Disease (PREVENT-AD, https://prevent-alzheimer.net/). Some of the data are publicly available (https://openpreventad.loris.ca/, and https://www.mcgill.ca/bic/neuroinformatics/omega). In compliance with the ethical and privacy policies stipulated in the PREVENT-AD study to protect the identity of the participants and to preserve their right to refrain to share part of their biological/imaging data openly, the full internal release of the dataset https://registeredpreventad.loris.ca/ can only be shared upon approval by the scientific committee at the Centre for Studies on Prevention of Alzheimer's Disease (StoP-AD) at the Douglas Mental Health University Institute. Detailed instructions for accessing the open and requesting access to the full internal release versions of the PREVENT-AD dataset can be found here: https://prevent-alzheimer.net/?page_id=1760&lang=en. For more details regarding the organization of the PREVENT-AD dataset please refer to Breitner et al.,50 and Tremblay-Mercier et al.,51. For further about getting access to the PREVENT-AD dataset please contact co-author Sylvia Villeneuve (sylvia.villeneuve@mcgill.ca). The Desikan-Killiany atlas parcellation is included in FreeSurfer version 5.3 (https://surfer.nmr.mgh.harvard.edu/fswiki/CorticalParcellation) and the ggseg package version 1.6.5 (https://github.com/ggseg). Centiloid data transformation was done by adapting a formula for our NAV4694 tracer following the steps described by Klunk et al.,71 and Rowe et al.,72. The normative NAV4694 data necessary for the centiloid validation can be found on the GAAIN website of the Alzheimer Association (https://www.gaain.org/centiloid-project).

Research involving human participants, their data, or biological material

Policy information about studies with human participants or human data. See also policy information about sex, gender (identity/presentation), and sexual orientation and race, ethnicity and racism.

Reporting on sex and gender	The sex of the participants was included as a covariate in all of the statistical analysis implemented on this work. The final sample included in the statistical analysis comprised 104 individuals, including 30 males and 74 females. No gender information was collected nor incorporated into the analysis.
Reporting on race, ethnicity, or other socially relevant groupings	The cohort used in this study mainly consists of highly educated, white, North-American participants, which should be considered when interpreting the generalizability of the results. Neither race nor ethnicity were included as variables of interest in any of the analysis presented here.
Population characteristics	Considering the importance of age and years of education for evaluating functional brain features and cognitive performance, these variables were included as covariates in all of the statistical analysis presented here. The mean age was 67.4 (SD = 4.9) years, and the mean years of education were 15 (SD = 3.1).
Recruitment	Participants were selected based on specific criteria aligned with the aims of the study. PREVENT-AD participants were required to: 1) have one parent or multiple siblings with an Alzheimer's Disease diagnosis, 2) be at least 60 years of age or between 55 and 59 if their age was >15 years younger than their first-affected relative's age at dementia onset, 3) have no history of major psychiatric or neurological disorders and 4) be rated as cognitively normal at the time of enrollment. Normal cognition was determined by having a score ≥ 26 in the Montreal Cognitive Assessment (MoCA) and a score of 0 in the Clinical Dementia Rating (CDR) scale.
Ethics oversight	This research projects was conducted in accordance with the principles of the Declaration of Helsinki for experiments involving human participants and was approved by the Institutional Review Board at McGill University (Protocol #A05-B16-11B and #A05-M55-11B). All participants provided informed written consent, and received a compensation to cover travel expenses and time

Note that full information on the approval of the study protocol must also be provided in the manuscript.

Field-specific reporting

Please select the one below that is the best fit for your research. If you are not sure, read the appropriate sections before making your selection.

☒ Life sciences ☐ Behavioural & social sciences ☐ Ecological, evolutionary & environmental sciences

For a reference copy of the document with all sections, see nature.com/documents/nr-reporting-summary-flat.pdf

Life sciences study design

All studies must disclose on these points even when the disclosure is negative.

Sample size	We included 124 participants from PREVENT-AD - a large cohort of asymptomatic older adults with familial risk of sporadic Alzheimer's disease dementia. No statistical methods were used to predetermine sample size, but our sample size is similar or larger to that reported in previous publications including multimodal imaging data (i.e. MEG, PET) in a similar population (López-Sanz et al., 2016; Nakamura et al., 2018; Wiesman et al., 2021).

Data exclusions	The data from 20 participants were discarded due to issues with MEG signal integrity (1 participant), PET data quality (1 participant), and unusable MEG data due to high-amplitude noise caused by ferromagnetic dental implants (18 participants).
Replication	We replicated our main analyses after identifying and removing outliers (based on Cook's distance). We were not able to replicate our analyses using an alternative cohort, as there is no other openly available dataset that includes all the multiple imaging modalities used here (MEG, MRI, Aβ and tau PET). We performed a predictive analysis to assess whether our findings in the preclinical phase of AD align with the changes in neurophysiological activity reported in advanced disease stages (MCI, AD). We found that our estimations of the magnitude of the shift from neurophysiological acceleration to slowing are in line with the reported effects in previous publications focusing on the later stages of the disease.
Randomization	No random allocation of participants into experimental groups was used in the present study. For the subset of between-subject analysis presented here, individuals were grouped based on the amount of amyloid and tau PET tracer binding in sensitive brain regions. Thresholds for the definition of amyloid and tau positivity were defined as two standard deviations above the mean amyloid and tau uptake estimated from the same brain regions in an independent sample of 11 young healthy individuals.
Blinding	Data collection and analysis were not performed blind to the conditions of the experiment, but group allocation was only implemented for the supplementary between-subjects analysis. In this analysis, group separation was based on predefined fixed thresholds for the levels of global Aβ and entorhinal tau PET tracer binding in sensitive brain regions, which were defined as 2 standard deviations above the mean of a group of 11 young individuals.

Reporting for specific materials, systems and methods

We require information from authors about some types of materials, experimental systems and methods used in many studies. Here, indicate whether each material, system or method listed is relevant to your study. If you are not sure if a list item applies to your research, read the appropriate section before selecting a response.

Materials & experimental systems

n/a	Involved in the study
☒	☐ Antibodies
☒	☐ Eukaryotic cell lines
☒	☐ Palaeontology and archaeology
☒	☐ Animals and other organisms
☒	☐ Clinical data
☒	☐ Dual use research of concern
☒	☐ Plants

Methods

n/a	Involved in the study
☒	☐ ChIP-seq
☒	☐ Flow cytometry
☐	☒ MRI-based neuroimaging

Magnetic resonance imaging

Experimental design

Design type	n/a
Design specifications	n/a
Behavioral performance measures	n/a

Acquisition

Imaging type(s)	Structural imaging
Field strength	3.0 Tesla
Sequence & imaging parameters	T1-weighted acquired using a MPRAGE gradient-echo sequence, 176 slices (1 mm slice thickness), TR = 2300 ms, TE = 2.98 ms, flip angle = 9°, FoV = 256x240x176 mm.
Area of acquisition	Whole-brain scan

Diffusion MRI ☐ Used ☒ Not used

Preprocessing

Preprocessing software	Freesurfer version 5.3
Normalization	Structural MRI data were only used during the preprocessing of MEG and PET data. Quantification of MEG and PET features were computed within each individual's anatomical space and therefore no normalization was used.

Normalization template: n/a

Noise and artifact removal: n/a

Volume censoring: n/a

Statistical modeling & inference

Model type and settings: n/a

Effect(s) tested: n/a

Specify type of analysis: ☐ Whole brain ☒ ROI-based ☐ Both

Anatomical location(s): We used the Desikan-Killiany atlas for parcellating the structural MRIs

Statistic type for inference: n/a

(See Eklund et al. 2016)

Correction: n/a

Models & analysis

n/a	Involved in the study
☒	☐ Functional and/or effective connectivity
☒	☐ Graph analysis
☒	☐ Multivariate modeling or predictive analysis